Summer 8-18-2017

Oyster Aquaculture Site Selection Using Landsat 8-derived Sea Surface Temperature, Turbidity, and Chlorophyll a.

Jordan Snyder
University of Maine, Orono, jordan.snyder@maine.edu

OYSTER AQUACULTURE SITE SELECTION USING LANDSAT 8 – DERIVED SEA SURFACE TEMPERATURE, TURBIDITY, AND CHLOROPHYLL A

By

Jordan Snyder

B.S. University of California, Davis, 2013

A THESIS

Submitted in Partial Fulfillment of the

Requirements for the Degree of

Master of Science

(in Oceanography)

The Graduate School

The University of Maine

August 2017

Advisory Committee:

Emmanuel Boss, Professor of Marine Science, Co Advisor

Damian Brady, Assistant Professor of Marine Science, Co Advisor

Andrew Thomas, Professor of Marine Science

OYSTER AQUACULTURE SITE SELECTION USING LANDSAT 8-DERIVED

SEA SURFACE TEMPERATURE, TURBIDITY, AND CHLOROPHYLL A

By Jordan Snyder

Thesis Advisors: Dr. Emmanuel Boss, Damian Brady

An Abstract of the Thesis Presented
in Partial Fulfillment of the Requirements for the
Degree of Master of Science
(in Oceanography)

August 2017

Remote sensing data is useful for selection of aquaculture sites because it can provide water-quality products mapped with no cost to users. However, the spatial resolution of most ocean color satellites is too coarse to provide usable data within many estuaries. The more recently launched Landsat 8 satellite has both the spatial resolution and the necessary signal to noise ratio to provide temperature, as well as ocean color derived products along complex coastlines. The state of Maine (USA) has an abundance of estuarine indentations (~3,500 miles of tidal shoreline within 220 miles of coast), and an expanding aquaculture industry, which makes it a prime case-study for using Landsat 8 data to provide products suitable for aquaculture site selection. We collected the Landsat 8 scenes over coastal Maine, flagged clouds, atmospherically corrected the top-of-the-atmosphere radiances, and derived time varying fields (repeat time of Landsat 8 is 16 days) of temperature (100 m resolution), turbidity (30 m resolution), and chlorophyll-a (30 m resolution). We validated the remote-sensing-based products at several *in situ* locations along the Maine coast where monitoring buoys and programs are in place. Initial analysis of the validated fields revealed promising areas for oyster aquaculture. The approach used and the data collected to date show potential for other applications in marine coastal environments, including water quality monitoring and ecosystem management.

ACKNOWLEDGEMENTS

Thank you Emmanuel Boss, Damian Brady, Andy Thomas and Carter Newell for guiding and instructing me. Thank you Ryan Weatherbee for patiently working with me and helping me with the satellite data processing. Thank you to Catherine Coupland, Nicolas DelPrete, Tiega Martin, Chris Rigaud, Matthew Grey, and Robbie Downs for your assistance maintaining the LOBO buoys at the Darling Marine Center. Thank you to Nils Haëntjens for assistance with data processing and editing. Thank you to Jocelyn Runnebaum and Kevin Staples for the helpful edits. Thank you to the SEANET project at University of Maine for providing LOBO buoy data and travel support. Thank you Dana Morse, Beth Bisson and Maura Thomas for support. Thank you Kelly, LeAnn and Ali for being spectacular lab mates, and thank you to my family for your continued encouragement.

TABLE OF CONTENTS

LIST OF TABLES

LIST OF FIGURES

LIST OF EQUATIONS

LIST OF ABBREVIATIONS

SST - Sea Surface Temperature

T – Turbidity

SPM – Suspended Particulate Matter

Chl a – Chlorophyll-a

AVHRR – Advanced Very High Resolution Radiometer

R_{rs} – Remote sensing reflectance

OSI – Oyster Suitability Index

DRE – Damariscotta River Estuary

CDOM – colored dissolved organic matter

NERACOOS – Northeastern Regional Association of Coastal Ocean Observing Systems

LOBO – Land/Ocean Biogeochemical Observatory

NTU – Nephalometric turbidity units

b – backscattering

b_{bp} – backscattering of particles

b_{bw} – backscattering of water

a_w – absorption of water

${a_p}^*$ – absorption of particles

a_g – absorption of dissolved substances

CHAPTER 1

INTRODUCTION

Oyster aquaculture of the American oyster, *Crassostrea virginica*, is an expanding industry in coastal Maine, USA, with landings worth $4.8 million dollars in 2015, up from $0.6 million in 2003 and increasing by 250% between 2011 and 2015 (Maine DMR commercial landings 2016, www.maine.gov/dmr). To meet the growing demand for high quality oysters, identification of new sites with the most optimal biophysical conditions for oyster growth is needed. To decrease the risk of choosing an unproductive site, it is crucial that growers have the right tools for site selection. Currently, the method for selecting a suitable site for bivalve aquaculture is largely based on proximity to existing sites or trial and error. These methods are inefficient because they may not consider the specific temperature and nutritional conditions needed for the species to grow, each of which affect how fast it takes to reach market size (Hawkins et al., 2013; Rheault & Rice, 1996). Recent advances in remote sensing techniques enable satellite imagery to help in site selection (e.g. Thomas et al., 2011). By visually inspecting information products calculated from processed Landsat 8 satellite images, estuaries that reach relatively warm temperatures (above 20°C), support high levels of chlorophyll in the summer (above 1 μg Chl L^{-1}), and exhibit low turbidity (below 8 NTU) can be efficiently identified as potential oyster growing areas.

The spatial resolution of standard global ocean color satellites (typically 1 km x 1 km) is too coarse to provide usable data within the many estuaries and embayments along coastal Maine where much of the suitable habitat for oyster aquaculture is located. The Thermal Infrared Sensor (TIRS) and the Operational Land Imager (OLI) are sensors on the Landsat 8 satellite, launched February 11, 2013. These sensors have both the spatial resolution (100 m for infrared data and 30 m for multi spectral visible data) and the necessary signal to noise ratio to provide useful temperature as well as ocean color derived products along the Maine coastline (Vanhellemont and Ruddick, 2014). In this paper, we used a combination of empirical and analytical approaches to derive temperature, turbidity and chlorophyll products from Landsat 8 Operational Land Imager (OLI) and Thermal Infrared Sensor (TIRS) data for the coast of Maine.

Although it was designed for terrestrial monitoring, Landsat 8 data can be used for marine applications if a reliable atmospheric correction is applied. An atmospheric correction is necessary for satellite remote sensing because in the visible wavelengths the signal observed by the satellite is reflected from gas and aerosol particles in the atmosphere (Mobley et al, 2016). We used the NASA software platform SeaDAS, and algorithms implemented within it, together with an empirical approach to derive chlorophyll and turbidity.

As with any instrument, there are limitations to using Landsat 8 imagery for coastal monitoring. Compared to satellites, such as AVHRR and MODIS, that have daily coverage, the temporal resolution of Landsat 8 coverage is low. The 16 day repeat coverage makes it insufficient to observe short-term changes (due to weather, storm events, etc.), but it is useful for describing patterns such as seasonal averages, which is informative for monitoring long-term conditions and relative spatial differences between sites. Additionally, cloud cover decreases the probability of clear overpasses; most of the images we retrieved come from summer and fall months (June through November) when there was the least amount of cloud cover. Fortunately, this is also the critical time of year for oyster aquaculture as it overlaps most of the growing season.

Ocean color measurements can be used to describe components of water quality, such as turbidity and chlorophyll-a (Chl *a*) concentration (O'Reilly et al., 1998). Algorithms have been developed that can estimate concentrations of these components by 1) retrieving radiant flux from the target surface, 2) correcting for the signal from the atmosphere, 3) transforming radiant energy collected by the satellite sensor into remote sensing reflectance ($\mathrm{R_{rs}}$), and 4) converting $\mathrm{R_{rs}}$ values into products.

Reflectance in the red wavelengths of light is used to estimate suspended particulate matter (Dogliotti et al., 2015; Vanhellemont and Ruddick, 2014), while reflectance in the blue and green wavelengths is used to estimate of Chl *a* biomass (a proxy of phytoplankton biomass) (Franz et al., 2015; Mobley et al., 2016). These methods have been used for monitoring in several sites around the world (Aguilar-Manjarrez and Crespi, 2013; Gernez et al., 2014; Radiarta et al., 2008; Thomas et al., 2011; Wang et al., 2010) to assess the impacts of turbidity and Chl *a* on aquaculture.

Optimal conditions for oyster growth have been determined primarily through the use of various types of ecophysical models. Habitat suitability models were first applied to the restoration of the American oyster, *Crassostrea virginica*, on the warm southeast Atlantic coast of the U.S. (Cake, 1983; Soniat and Brody, 1988; Barnes et al., 2007). These models considered bottom substrate and suitable salinities to maximize oyster survival in relation to siltation and protozoan parasites. More recently, Radiarta et al. (2008) used satellite imagery of Chl *a* and sea surface temperature (SST), and weighted bio-physical, social-infrastructural constraint criteria and a model builder in ARC GIS to identify sites best suited for hanging culture of scallops (i.e. high food availability, minimal distance to support services, and favorable depth). Carrasco and Baron (2010) used satellite imagery to map temperatures which defined the potential range for Pacific oyster populations in South America. Thomas et al. (2011) used satellite-derived SST and Chl *a* in Mont Saint-Michel Bay, France, to predict mussel growth based on a dynamic energy budget model. Statistical models relating organism growth, biomass and economic yield illustrate the importance of site specific environmental variables (water velocity, food concentration) on farm yields (Pérez-Camacho et al., 2014). Powell et al. (1992) and Hoffman et al. (1992) modeled American oyster filtration rate and growth as a function of animal size, water temperature and total particulate matter, with a negative effect at high suspended loads, although selection for organic matter by the oyster when producing pseudofeces was not considered (Newell and Jordan, 1983). Gernez et al. (2014), used 300m pixel-size SPM distributions derived from MODIS to provide a spatial picture of the impact of SPM concentration on oyster-farming sites.

Crassostrea virginica is somewhat unusual in that its filtration rate is a strong function of temperature from 8°C to a maximum at 30°C compared to other bivalves where the filtration rate is relatively independent of water temperature (Loosanoff, 1958). Therefore, temperature is of primary importance in site selection for oyster aquaculture in the relatively heterogeneous and strongly seasonal sea surface temperature regime of the colder Maine waters. Bivalve feeding and growth is also a positive function of phytoplankton concentration (Hawkins et al., 2013), so Chl *a* is considered the next most important factor for site selection. In general, total suspended particulate matter has a negative effect on bivalve growth by diluting the organic matter at high levels (Widdows et al., 1979; Barille et al., 1997). In some areas, there is a relatively high proportion of inorganic particles in resuspended sediments, and in others, sediments consist of both inorganic matter and particles that contain chlorophyll. For bivalves, the proportion of phytoplankton in the suspended particles is a key aspect of site suitability, (Newell et al., 1989).

Another important factor in oyster site selection is water velocity, which delivers food to populations of oysters at commercial-scale densities. Congleton et al. (1998) developed a GIS system that included water velocity and intertidal elevation to predict optimal locations for clam (*Mya arenaria*) mariculture. Within a coastal bay, ShellGIS used the growth model Shellsim to predict oyster growth and yield as a function of water quality (temperature, salinity and food concentration), husbandry and seeding density, and water velocity on a 50 m farm scale (Newell et al., 2013; Hawkins et al., 2013). Water velocity is not a limiting factor in the coast of Maine where tidal amplitudes and currents are large. Hence, the primary screening tools of temperature, chlorophyll *a*, and turbidity are effective tools to identify suitable locations on the bay scale, and provide novel opportunities for mapping potential zones for aquaculture development over large coastal regions such as Maine or Alaska in the U.S.

We present and demonstrate a methodology to obtain SST and calibrated water quality products from the TIRS and OLI sensors on board Landsat 8, and validate them with measurements in coastal Maine waters. We computed uncertainties based on match-ups between local data and that derived from satellites and discuss how temporal and spatial sampling and adjacency effects affect the accuracy of remote sensing products. These processed satellite products were then used for mapping oyster aquaculture sites, and proved useful because they verified good conditions at existing farms, and revealed other locations along the coast of Maine with similarly optimal conditions that could be developed for oyster aquaculture.

CHAPTER 2

METHODS

2.1. Study Area

The coast of Maine includes a series of fjards (shallower and broader fjords) and jagged embayments carved by receding glaciers during the Pleistocene epoch. *In situ* samples were collected and ocean monitoring buoy systems were maintained in two of these estuaries, the Damariscotta River and Harpswell Sound, over the course of several years and we used them here to validate Landsat-8 derived products on the Maine coast (triangles on Figure 1). We chose to focus on the Damariscotta River because it has existing aquaculture operations (currently 75% of the oysters produced in Maine, (Maine DMR, 2015)) and suitable sampling access. The Damariscotta River Estuary is 29 kilometers long, has a mean summer flushing time of 4 to 5 weeks, and is dominated by strong tides with amplitudes of up to 3.35 m (McAlice, 1977). Sediment resuspension in this estuary is highest at low tide, and lowest at high tide. The estuary is highly saline, ranging from 25 to 32.5 psu, with a small amount of fresh water input from Damariscotta Lake into Salt Bay at its northern reach. The substrate is a soft, muddy bottom composed of clay to sandy silts with an average depth of 15.25 m. These attributes make the Damariscotta River an ideal place for growing market-size oysters and other bivalve species, and make it an excellent reference point for expanding the aquaculture industry along the coast of Maine.

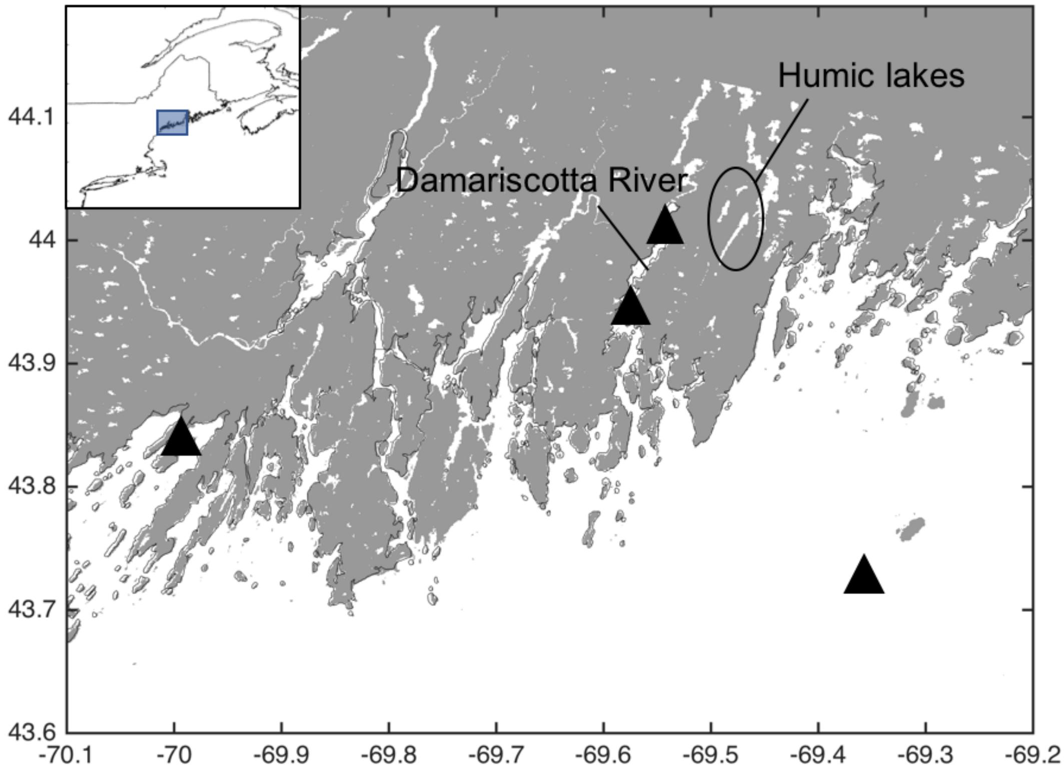

Figure 1. Map of mid-coast Maine, USA. Triangles indicate locations of validation buoys. Freshwater lakes used for the atmospheric correction are located at approximately 44'N, -69.5'E.

2.2. Processing of Sea Surface Temperature

All applicable raw data from Landsat 8 was downloaded from the USGS Earth Explorer website from the period 2013 to 2016 (USGS, 2016). To calculate SST, we used brightness temperature values from Landsat 8's Thermal Infrared Sensor (TIRS) Band 10. There are stray light issues associated with the two TIRS bands (Band 10 and Band 11) due to the curvature of the optical lens (Montanaro et al., 2014). Of these two bands, we chose to use thermal Band 10 because it has lesser issues of the two (see Discussion section). Each image was processed in the NASA SeaDAS platform up to level 2 to retrieve latitude and longitude arrays, a geo-registered image, and the associated land/cloud mask (georeferencing is maintained, as it is provided from USGS).

Regressions between coincident atmospherically corrected AVHRR satellite derived SST and that derived from Landsat 8's brightness temperature were used to create an SST product for the Landsat 8 imagery (similar to Thomas et al., 2002). This regression process, de-facto, acts as the atmospheric correction for the Landsat SST product 1) assuming that the atmosphere does not change in the time interval between AVHRR and Landsat overlapping image and 2) the atmosphere is homogenous across the Landsat scene. Example data from this procedure are displayed on Figure 2 below. Of the four to eight AVHRR images captured on the same day as Landsat 8, we subjectively chose the image with the least amount of cloud cover and poorly masked pixels, best geolocation, and cleanest SST patterns, for the regression (see Appendix A for detailed description). The data for the regression was selected from cloud free and offshore areas to accommodate the lower AVHRR resolution (1 km versus Landsat 8 100 m resolution). The best results were achieved using cloud free areas with a high dynamic range in SST. The resulting regression equation between the signal of Landsat's Band 10 and the AVHRR-based temperature was then applied to provide SST for the full resolution Landsat 8 image.

In general, there are approximately four AVHRR images per day. Due to changing cloud cover and orbit configuration between available AVHRR images, it was sometimes necessary to use an image more distant in time (but less cloudy) from the Landsat 8 overpass, despite a temporally more proximate one being available. However, because Gulf of Maine SST patterns change slowly (less than 0.4^{o}C over 12 hours at buoy 44005, www.neracoos.org), we consider this an acceptable tradeoff to maximize the number of quality AVHRR pixels that will be used in the regression. The mean offset time between the Landsat 8 and AVHRR overpasses was 6.8 hours, with a minimum offset of 2.3 hours, maximum offset of 30.2 hours, and a standard deviation of 5.8 hours. The entire area of overlap between AVHRR ocean pixels and Landsat 8 ocean pixels is used for most scenes. Landsat 8 images were subsampled to every 10th pixel in both x and y dimensions to reduce the data volume for the regressions, and AVHRR images were resampled to match the 30m (interpolated from 100m) resolution of the Landsat B10 using nearest neighbor resampling in MATLAB. Depending on the distribution of clouds, the regression area was restricted to areas without cloud contamination (or poorly masked clouds) in some instances. Cloud and land were dilated by two pixels in the AVHRR image to reduce occurrences of cloud ringing artifacts and nearshore land contamination. The regression process was iterative. After each iteration, all Landsat 8 and coincident AVHRR pixels that were greater than one standard deviation from the linear best fit line of the relationship were removed and the regression was re-calculated with the remaining data. The iteration process was repeated until the Pearson correlation coefficient for the two datasets stabilized or started to worsen (which is due to uncertainties in the approach). The final regression equation was then applied to each Landsat 8 B10 pixel at the full 30 m resolution to obtain a Landsat SST image.

2.3. Ocean Color

Ocean color multispectral data, which responds to the effects of oceanic particles and dissolved matter, are measured from space by the Operational Land Imager (OLI) radiometer on board Landsat 8. The radiance measured includes contributions from the target (the surface water column), the air water interface, and the background (particles and gases from nearby pixels and particles in the atmosphere) (Mobley et al., 2016). To obtain information on the oceanic constituents, the atmospheric contribution to the signal needs to be removed (a process known as 'atmospheric correction' see below). From the corrected water-leaving radiance, we computed the reflectance (denoted as $\mathrm{R_{rs}}$) from which the products of turbidity and Chl *a* are derived.

2.4. Atmospheric Correction for $\mathbf{R_{rs}}$

Given the low turbidity in our area of investigation (see Section 2.5 below), we chose to use a combination of the Near Infrared (NIR) and Short Wave Infrared (SWIR) channels for atmospheric correction in SeaDAS. The NIR was important to use because of its higher signal/noise ratio (NIR bands had ratios of 6 and 7 while SWIR bands had ratios of 9 and 10) in low turbidity waters, and the SWIR was important because it has the strongest absorption for water which helps differentiate in-water sediments from atmospheric aerosol particles (Franz et al., 2015; Pahlevan et al., 2014). Applying this atmospheric correction over a scene resulted in a per-pixel correction, each with its own angstrom coefficient. The angstrom coefficient is the slope of the spectral aerosol optical thickness, which is derived relative to a reference wavelength (usually 443 nm/865 nm as output from SeaDAS). We adjusted this coefficient because the automatic per-pixel retrievals provided by SeaDAS resulted in negative values in several freshwater areas that were black body targets for our atmospheric correction scheme and should have near-zero or positive retrievals. The primary reason for adjusting the angstrom is that the aerosol models used for processing data from satellites such as SeaWiFs and MODIS (Ahmad et al., 2010), do not represent the aerosol conditions for our study area, the coast of Maine (Pahlevan et al., 2017). We then chose a single angstrom coefficient per scene (from within the distribution of inverted angstrom values), by requiring that the minimal value of $\mathrm{R_{rs}}(443)$ in a scene, measured in a very humic lake, be near zero. Most freshwater lakes on the coast of Maine are humic and have high levels of chromophoric dissolved organic matter, CDOM, which gives them a brown hue and attenuates light quickly (Roesler and Culbertson, 2016; Rasmussen, 1989). Several freshwater lakes with high CDOM within our study region (Muddy Pond, Biscay Pond, and Damariscotta Pond circled in Fig. 1) were selected as suitable reference targets to correct the entire Landsat 8 scene. In each individual satellite image, the darkest lake (where $\mathrm{R_{rs}}(443)$ is near zero) was used to determine angstrom coefficient. Analysis of a sample of water from one of these lakes verified that the expected $\mathrm{R_{rs}}(443)$ is zero within the uncertainty of the measurement (Appendix Table B1). We subsequently applied the retrieved angstrom in SeaDAS to the entire scene to recalculate $\mathrm{R_{rs}}$ at every wavelength. $\mathrm{R_{rs}}$ values were then used to compute turbidity and chlorophyll.

2.5. Retrieval of Turbidity

Turbidity, T, (note that 1 g L^{-1} of SPM is equivalent, within the range of values found in our study area, to a turbidity of 1 NTU (Pfannkuche and Schmidt, 2003)) was calculated over the entire satellite scene using atmospherically corrected $R_{rs}(655)$ and the following equation from Nechad et al. (2010):

$$T = A^{\rho} \frac{\rho_w}{1 - \rho_w / C^{\rho}} [gm^{-3}] \qquad (1)$$

where $\rho_w = R_{rs}(655) * \pi$ and ρ_w is the atmospherically corrected and derived water leaving reflectance, A^{ρ} = 289.1 and C^{ρ} = 16.86 (Nechad et al., 2010).

2.6. Retrieval of Chlorophyll-a

Chl a was calculated using the standard OC3 algorithm (O'Reilly et al., 1998) from the NASA Ocean Biology Processing Group, using the above-calculated R_{rs}:

$$\log_{10}(chlor\_a) = a_0 + \sum_{i=1}^{4} a_i \log_{10}\left(\frac{R_{rs}(\lambda_{blue})}{R_{rs}(\lambda_{green})}\right)^i \qquad (2)$$

where $\mathrm{a_0}$ and $\mathrm{a_i}$ are sensor specific coefficients, and $\mathrm{R_{rs}(\lambda_{blue})}$ and $\mathrm{R_{rs}(\lambda_{green})}$ are the greatest of values from 443>483 and 555 nm, respectively, on the OLI sensor aboard Landsat 8 (NASA, 2016). (Note: SeaDAS applies coefficients to convert broad band Landsat 8-based $\mathrm{R_{rs}}$ to 11nm narrow bands for which this equation was developed).

2.7. Validation with *in situ* data

Validation was carried out for physical and biogeochemical parameters (SST, turbidity, and Chl a) using data from water samples and three oceanographic buoy observing systems. Historical data was downloaded from the NERACOOS (Northeastern Regional Association of Coastal Ocean Observing Systems) buoys E01 and I01 operated by the University of Maine, Orono, in the Gulf of Maine, a Land/Ocean Biogeochemical Observatory (LOBO) buoy at Bowdoin College in Harpswell Sound, and two LOBO buoys at the University of Maine's Darling Marine Center in the Damariscotta River (Fig. 1, NERACOOS Buoy I01 not pictured). The LOBO buoys were equipped with sensors that remain at a depth of 1.5 meters and maintained and cleaned to prevent biofouling every two weeks. Temperature data were collected from all three observing systems and compared to Landsat 8 SST. A total of 52 matchups were identified originating from 31 clear overpasses from 2013 to 2016.

In situ turbidity was used to validate satellite-derived turbidity during eight overpasses in 2015 and 2016. Data were collected from the UMaine LOBO buoys in the Damariscotta River, and were measured by a WET Labs WQM sensor capable of measuring turbidity from 0 – 25 NTU (that measure light scattered in the back direction at a 20 nm bandwidth around 700 nm). This sensor was vicariously calibrated against a Hach turbidity sensor (which is an ISO 7027:1999 turbidity standard). The buoy data were corrected by a regression between Hach turbidity samples and the LOBO turbidity with a slope factor of 1.58 (Appendix Table B2).

In situ Chl a was used to validate satellite-derived Chl a during the same eight overpasses in 2015 and 2016. *In situ* Chl a data were measured by the Damariscotta River LOBO buoys' WET Labs fluorescent sensor capable of measuring Chl a concentrations from 0 – 50 μg L^{-1}. The buoy data was corrected by a regression between extracted Chl a samples and the LOBO Chl a with a slope factor of 1.71. Water samples were collected in triplicate, at the surface, and in opaque bottles within 30 minutes of each overpass and filtered for extraction on a Turner 10 AU fluorometer per standard protocol (Holm-Hanson and Riemann, 1978).

2.8. Satellite Imagery for an Oyster Suitability Index

An Oyster Growth Suitability Index was designed using the satellite-derived SST, turbidity, and Chl a. A weighting and indexing procedure of these three physical parameters described ideal, moderate, and poor conditions for growing market sized oysters in surface culture. The criteria for the index were chosen based on published studies of environmental effects on oyster growth, recognizing that the concentration of organic detritus, known to be an important component of oyster diet, was not available. Temperature is the most important variable in oyster growth, especially in the cold waters of coastal Maine since it controls the filtration rate of oysters (and therefore given an importance weight factor of 80%; Loosanoff, 1958; Hoffmann et al., 1992; Ehrich and Harris, 2015). Oyster clearance of algae is a positive function of algae concentration, as large amounts of pseudofeces are produced at high algal concentrations. Because of this, we weighted Chl *a* at 15%, with poor conditions being less than 1 μg L^{-1} or greater than 10 μg L^{-1}, moderate conditions being 1 to 3 μg L^{-1}, and ideal conditions as to 10 μg L^{-1} (Epifanio and Ewart, 1977; Hawkins et al., 2013). Turbidity, as estimated by suspended particulate matter, has a negative effect on oyster feeding at high concentrations, by diluting algal cells with largely inorganic matter. Haven and Morales-Alamo (1966) observed large amounts of pseudofeces production by Eastern oysters at concentrations of suspended particulate matter above 10 mg L^{-1}, thus we gave turbidity a weight of 5% and designated poor conditions as greater than 10 μg L^{-1}, moderate conditions between 8 and 10 μg L^{-1} and ideal conditions under 8 μg L^{-1}. Hoffman et al. (1992) also modeled oyster filtration as a positive function of water temperature and a negative function of high suspended loads.

These relative weights were chosen as a starting point for the index and could be refined in future iterations to optimize the index (Gong et al., 2012), by doing a sensitivity analysis of the relative importance of the factors concomitant with growth measurements and growth model outputs. The resulting Oyster Suitability Index is the sum of the weighted conditions on a scale from 0 to 1, where pixels with a value of 1 represent waters where an oyster is likely to grow to market size within 2 years:

$$OSI = \sum_{i=1}^{n} SI_i \times w_i \quad (3)$$

where SI_i is the value of the environmental variable i, w_i is the weight of the variable i, and n is the number of environmental variables. We combined images from each year during the same month to create a monthly averaged index. Note: this index does not include information about site closures, bottom depth, or residential restrictions. Future work should include this information for a more comprehensive index.

CHAPTER 3

RESULTS

3.1. Satellite retrieved validation with *in situ* data

The Landsat 8 brightness calculation correlated well with *in situ* temperatures (RMSD is 0.82 °C, RRMSD is 4%, r^2= 0.94) with, on average, 1°C higher SST values than those measured by the buoy sensors, especially in warmer waters (Figure 2, 3). However, variability of the buoy measurements is larger at higher temperatures when horizontal gradients in temperature were also larger.

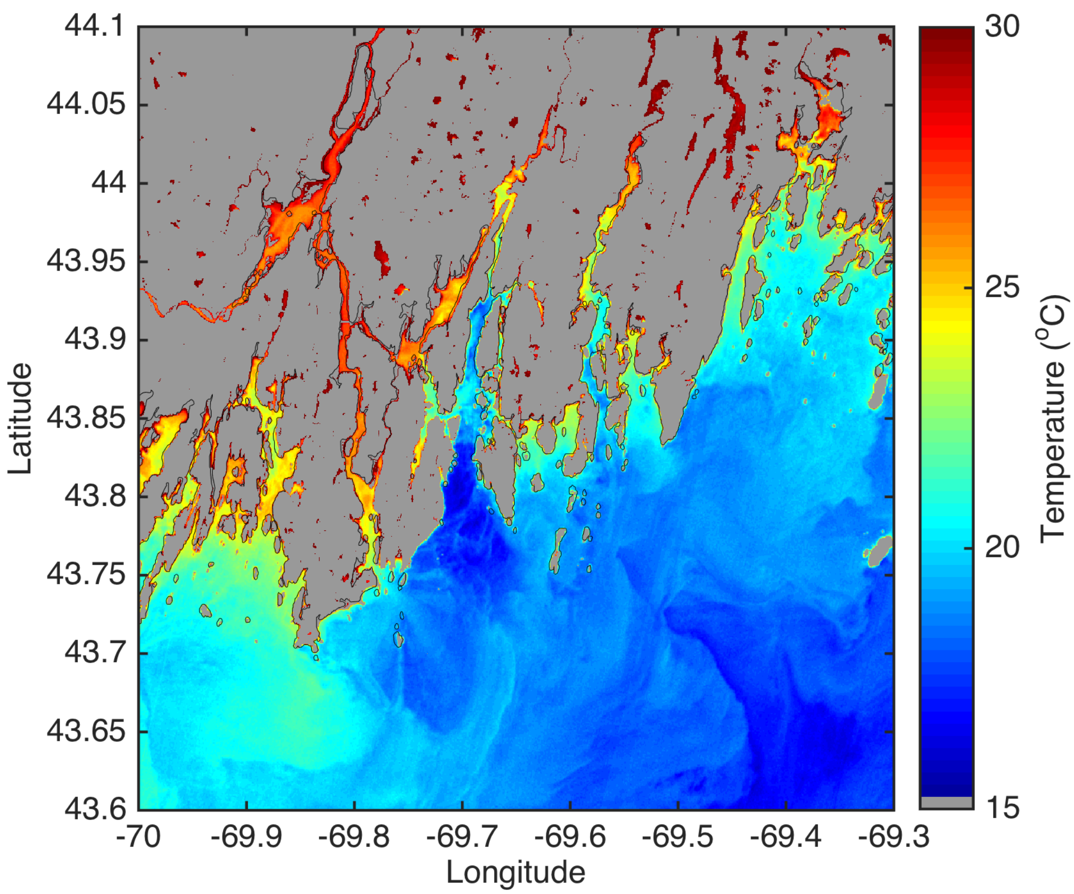

Figure 2. Landsat 8-derived Sea surface temperature map of mid-coast Maine on July 14, 2013. Spatial resolution is 30 meters (interpolated from 100 meters).

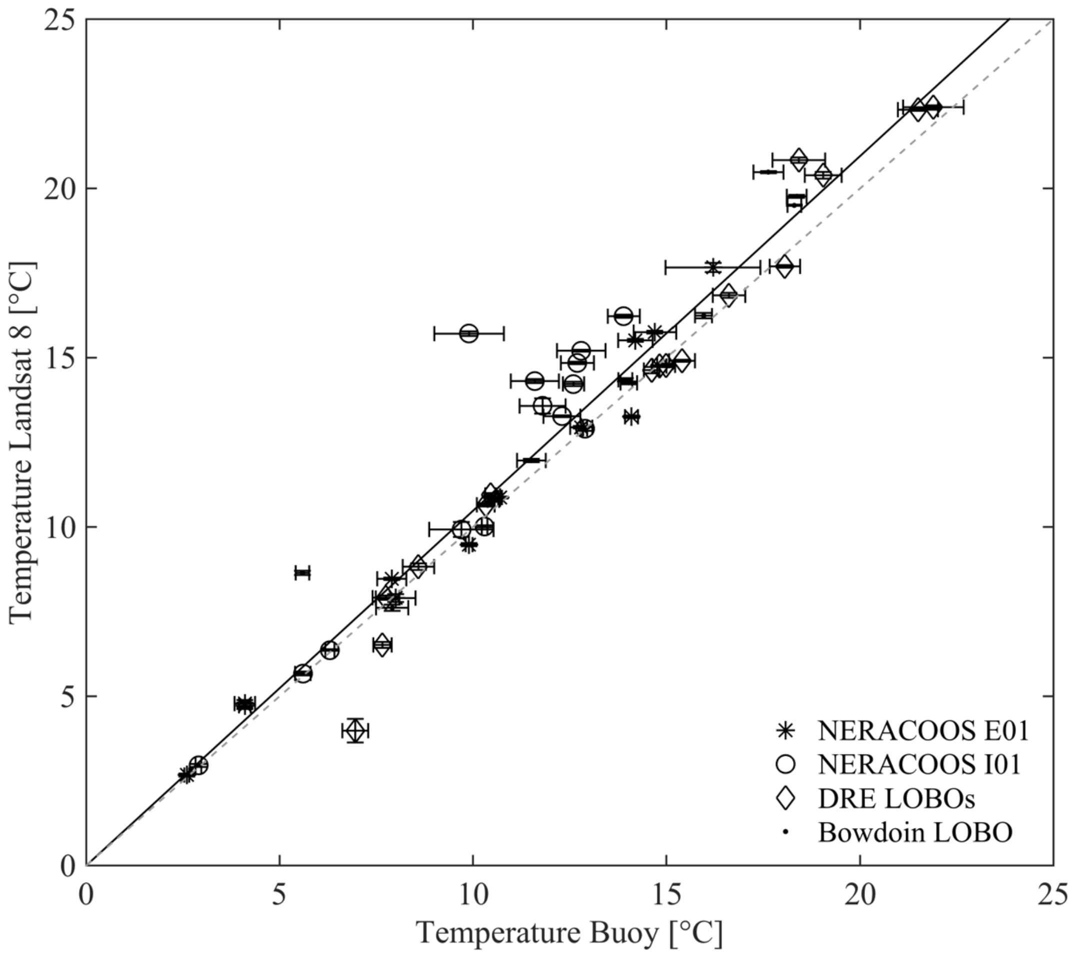

Figure 3. Type II linear regression for match-ups between Landsat 8 sea surface temperature and sea surface temperature measured by oceanographic buoys. Different symbols represent measurements by the three different observing systems. Vertical error bars are the standard deviation about a 5x5 pixel box centered at the *in situ* measurement. Horizontal error bars are the standard deviation of daily temperature at each buoy. Root mean square error is 0.82 °C, root mean square relative difference is 4%, r^2= 0.94 and the grey line is 1:1.

The Landsat 8 turbidity estimates correlated well with in situ turbidities (RMSD 0.49 NTU, RRMSD 3%, max absolute deviation is 0.96 and maximal relative deviation is 15%, r^2 = 0.88), with an uncertainty of

0.5 NTU, on average (Figure 4, 5). Uncertainties are larger at higher turbidities for both the buoy and the satellite algorithm.

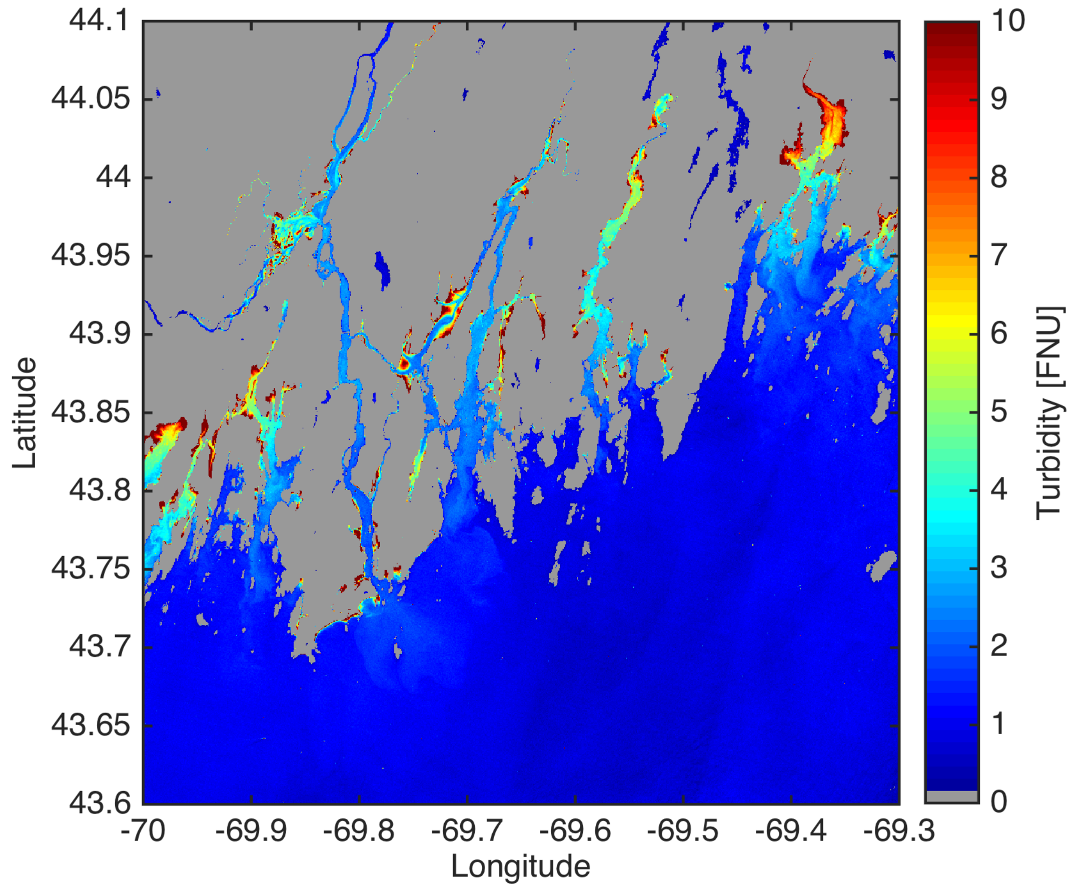

Figure 4. Landsat 8-derived turbidity along mid-coast Maine on July 14, 2013. Spatial resolution is 30 meters.

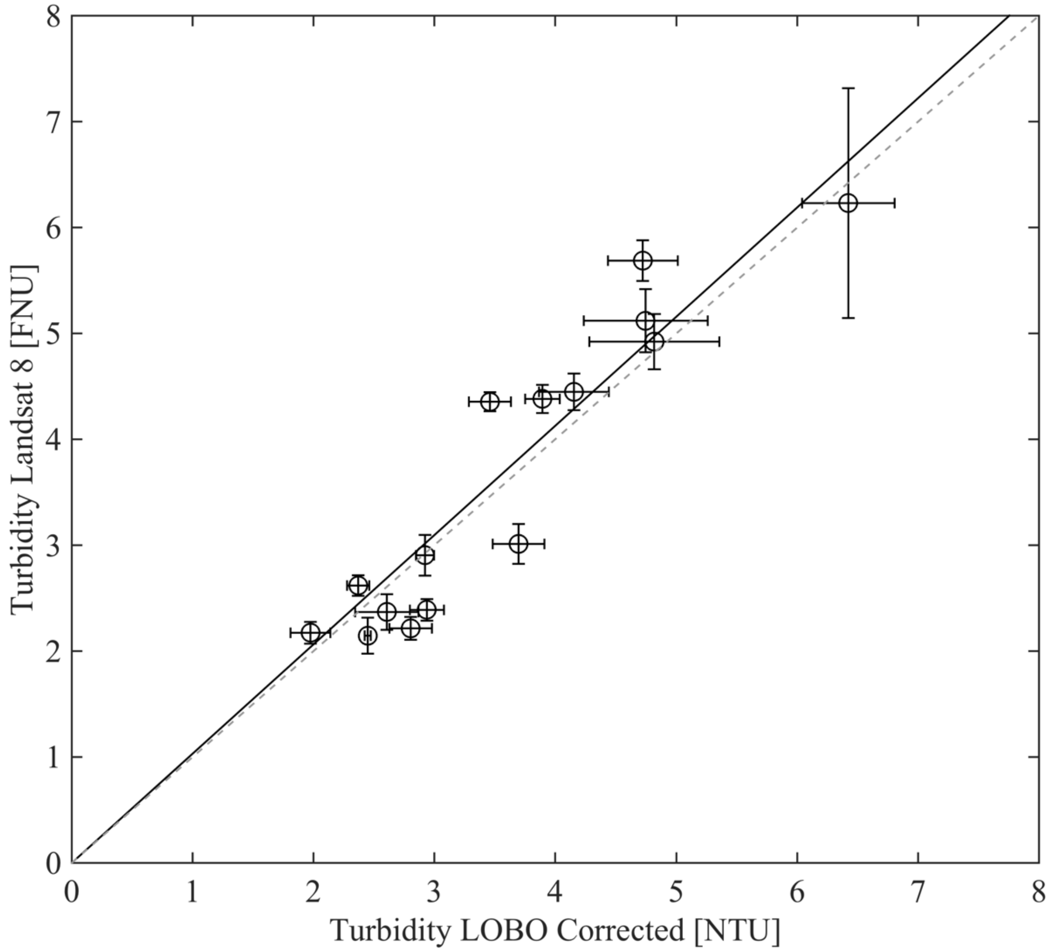

Figure 5. Type II linear regression between Landsat 8 turbidity and turbidity measured by LOBO buoys. Vertical error bars are the standard deviation about a 5x5 pixel box centered at the *in situ* measurement. Horizontal error bars are the standard deviation of turbidity for four hours at each buoy. Root mean square error between the two data sets is 0.49 NTU, root mean square relative difference is 3%, max absolute deviation is 0.96 and maximal relative deviation is 15%, $r^2 = 0.88$ and the grey line is 1:1.

Landsat-8 based chlorophyll did not correlate well with *in situ* Chl *a* (RMSD is 1.75 μg Chl L^{-1}, RRMSD is 110%, max absolute deviation is 3.14 μg Chl L^{-1}, max relative deviation is 156%, $r^2 = 0.31$). Below 5 μg L^{-1}, the OC3 algorithm produced higher Chl a values than those measured by the buoy sensors (Figure 6, 7). Above 5 μg L^{-1}, the buoy measurements were higher than the satellite-derived Chl a. Uncertainties are larger at higher Chl *a* for the buoys and the satellite algorithm. Out of the three parameters derived from Landsat 8, this algorithm has the highest relative deviation of 156%, with an average relative difference of 110%, which is significantly worse than the average relative difference of 30% for chlorophyll algorithms in the open ocean (but see Discussion).

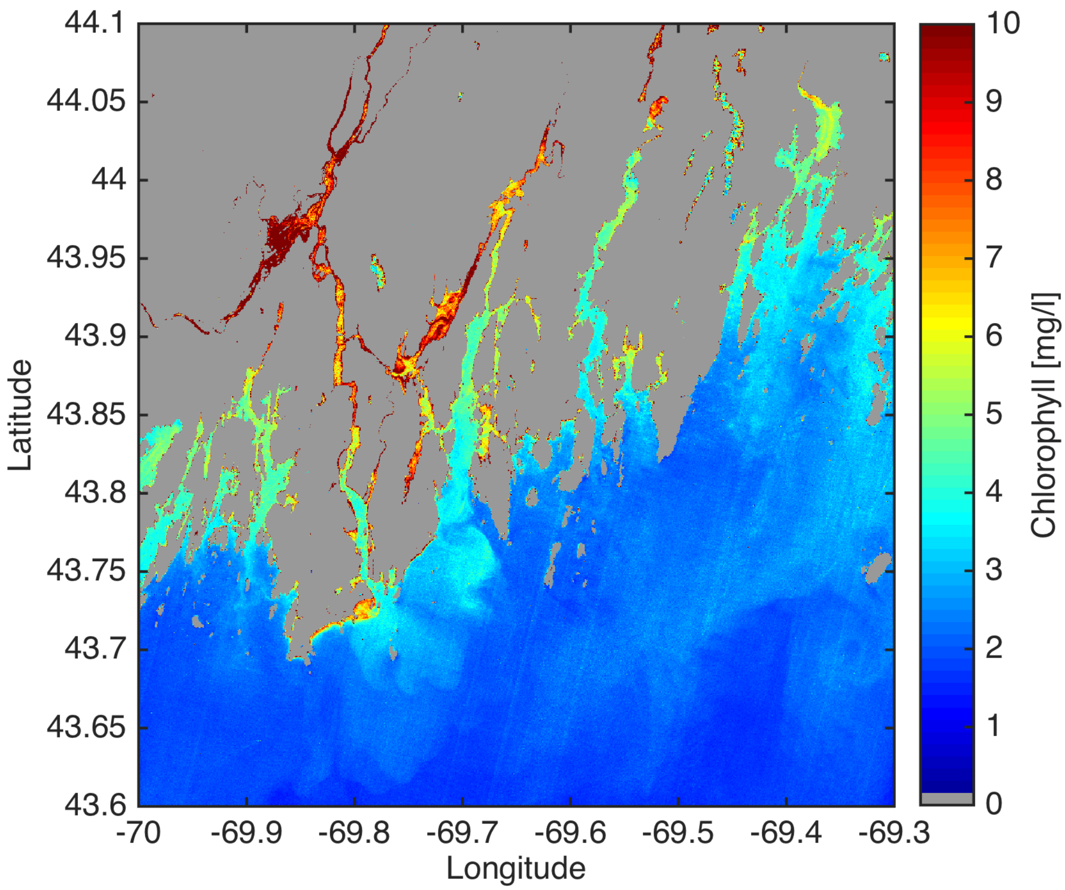

Figure 6. Landsat 8-derived chlorophyll *a* along mid-coast Maine on July 14, 2013. Spatial resolution is 30 meters.

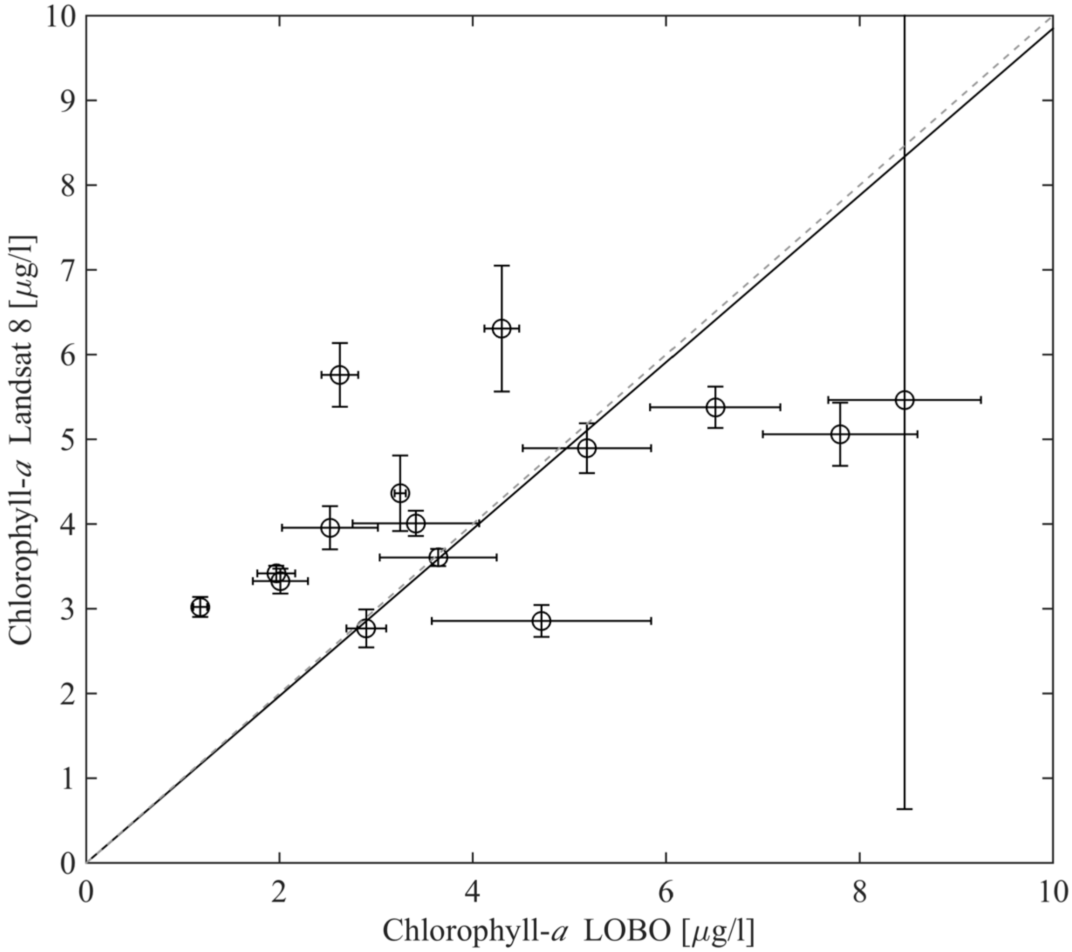

Figure 7. Type II linear regression between Landsat 8 chlorophyll-a and chlorophyll-a measured by LOBO buoys. Vertical error bars are the standard deviation about a 5x5 pixel box. Horizontal error bars are the standard deviation of chlorophyll-a for four hours at each buoy. Buoy chlorophyll-a was corrected by chlorophyll extraction samples. Root mean square error is 1.75 µg Chl L^{-1}, root mean square relative difference is 110%, max absolution deviation is 3.14 µg Chl L^{-1}, relative deviation is 156%, r^2= 0.31 and the grey line is 1:1.

3.2. Satellite Imagery for Oyster Growth Conditions

Monthly maps of an Oyster Suitability Index (Figure 8) were created using averaged monthly satellite images (Appendix C). Most existing oyster aquaculture areas (indicated by red stars on Fig. 8) fall within the highest suitability index during the month of July. Areas colored bright yellow indicate sites that are optimal for fast growing juvenile oysters (high temperature, low turbidity, and moderate Chl a). Areas in green indicate sites that are moderately suited for growing oysters, and areas in blue indicate waters that are least suitable for oyster growth. Suitability maps for August and September exhibit a similar pattern of ideal, moderate, and poor growing areas as the map for July (Fig. 8), but, in general, with slightly lower values due to colder temperatures (average monthly temperatures were highest during July). The Oyster Suitability Index map provides two important findings: 1) it confirms the Damariscotta River as a suitable place to grow oysters in aquaculture and therefore an important test and verification site for using remote sensing tools, and 2) it maps many new locations along the coast that host similar conditions (Appendix Table B2).

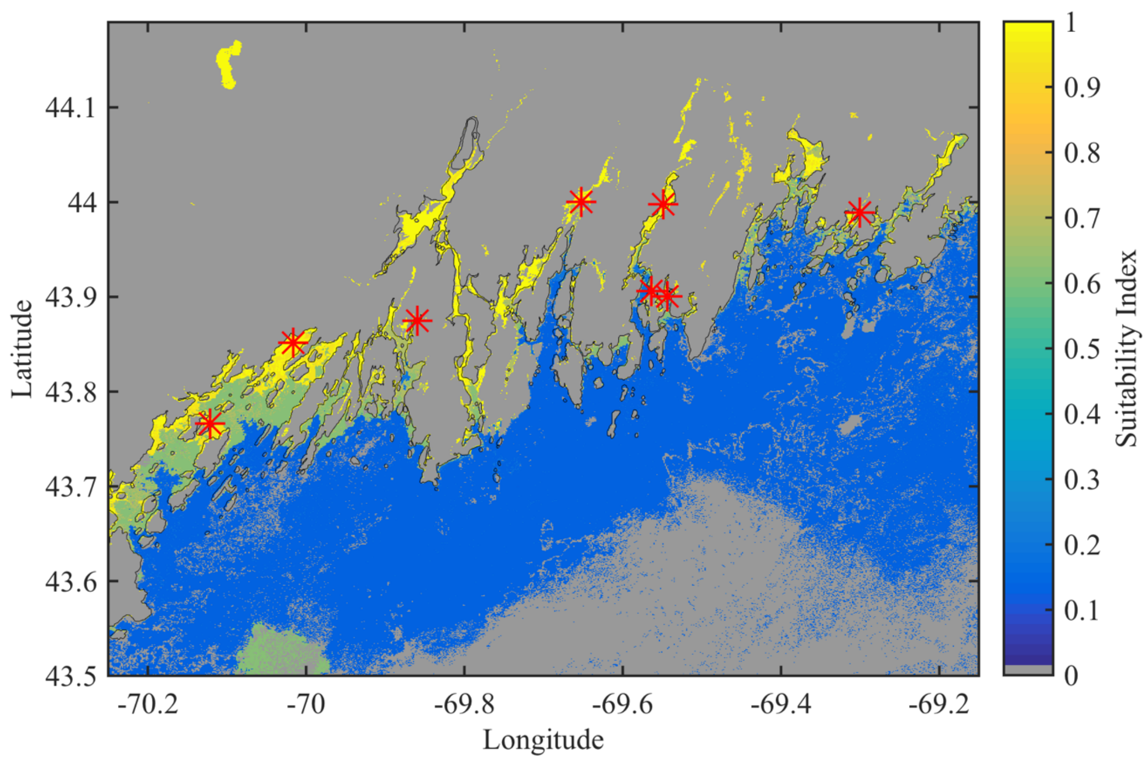

Figure 8. Oyster suitability map based on physical oceanographic parameters: sea surface temperature, turbidity, and chlorophyll-a. Map is an average of all images in the month of July. Yellow areas indicate ideal conditions, green areas indicate moderate conditions, and blue areas indicate poor conditions. Red stars indicate existing oyster farms. Index criteria is given in Appendix Table C, standard deviation of averaged parameters in July are given as figures in Appendix D.

CHAPTER 4

DISCUSSION

4.1. Satellite Imagery

The correspondence between the Landsat 8 satellite derived products and *in situ* measurements demonstrates the capability of generating SST, turbidity, and Chl *a* maps along the jagged coast of Maine. While these data show encouraging results, there are several factors from our study that could improve the present algorithms. Stray light issues arise if the temperature from an object outside of the field of view of the imager affects a pixel within the field of view. Fortunately, most water along the coast of Maine is vigorously tidally mixed (~3 m tidal range), and thus data from the center of channels can be used to infer the SST concentrations throughout those channels (Thornton and Mayer, 2015). Within the estuaries, however, a TIRS pixel (which is three times as wide as an OLI pixel) next to land may be incorrectly colder (if the land is colder) or warmer (if the land is warmer). However, the match-ups with temperature and turbidity products suggest adjacency and stray light have not degraded the data significantly, and differences are likely due to noise as opposed to systematic bias.

4.2. Limitations in Validation Process

Validation of Landsat 8 imagery with *in situ* measurements is necessary to assess the accuracy of the algorithms for retrieving bio-physical products. Some of the discrepancy between *in situ* and satellite matchups can be explained, while others require further investigation. One reason that Landsat 8 SST values may be higher than most buoy measurements (Fig. 3) is because the SST estimates come from light emitted from the top few micrometers of the sea surface, while the buoy sensors are located about 1.5 m below the surface. In the day time images, the subsurface water is likely cooler than the surface skin due to physical and environmental factors (Padula et al., 2010; Donlon et al., 2002; Ward, 2006).

Despite this bias, the Landsat 8 SST (derived by regressing with AVHRR) performed well along the coast of Maine (Fig. 3) and our results suggest that our approach could be used as a tool for measuring SST where high spatial resolution is desired.

A vigorous semi-diurnal tide characterizes the Damariscotta River and delivers shelf water into the upper reaches of the estuary. The tidal cycle was evident in the daily turbidity signal (not shown) from the LOBO buoys: at low tide, there are elevated levels of turbidity whereas at high tide there is less turbidity (due to the increase in turbidity from the mouth to the end of the estuary). The horizontal error bars in Figure 5 represent the variability during a four-hour period around each satellite overpass time, and highlight the importance of simultaneous sampling for *in situ* - satellite matchups. The turbidity algorithm performs well within our uncertainties in this context.

Landsat 8 Chl *a* often differs significantly from the LOBO buoy measurements. There are significant uncertainties associated with both measurement techniques (Cullen, 2008). Landsat 8 Chl *a* is retrieved from $\mathrm{R_{rs}}$ using an algorithm calibrated in the open ocean, whereas the LOBO buoys measure Chl *a* fluorescence which is regressed against water samples. Estimating Chl *a* from fluorescence is the most common way to measure Chl *a* but is affected by several processes that contribute to uncertainty. These include changes in fluorescence yield due to variability in the algal taxonomy, nutrient stress, and photo-acclimation, to name a few (Cullen, 1982). In addition, concentrations of phytoplankton have been observed in the Damariscotta River to vary on time scales of hours (Thompson and Perry, 2006).

Non-photochemical quenching (NPQ; when phytoplankton decrease their fluorescence at a maximum light harvesting level, e.g. Cullen, 1982) contributes to variability. However, we find nighttime measurements to be comparable to daytime measurements (Appendix Fig. B.1) for the Damariscotta River. Therefore, the offset in Chl *a* is likely not due to errors induced by NPQ. Another potential error is associated with the OC3 algorithm, which estimates Chl *a* as a ratio of R_{rs} in the blue and green channels.

The blue channel is especially affected by colored dissolved organic material (CDOM). Independent changes of CDOM will affect the OC3 chlorophyll estimate (Siegel et al., 2005). Along the coast of Maine, where there are coastal forests and marshes, CDOM is in high concentration and variable (Roesler & Culbertson, 2016). In coastal areas and estuaries rich in CDOM it is likely that absorption by dissolved organic matter would bias the OC3 algorithm. It is likely that a local algorithm that takes local CDOM concentration into account, could improve Chl *a* retrievals from Landsat 8.

4.3. Oyster Suitability Index

The Oyster Suitability Index provided in this paper is intended as a supplement to other tools that determine optimal oyster growing areas. Firstly, the satellite images provide only a climatological monthly snapshot of coastal temperature products, which provides less temporal resolution than a comprehensive day degree model for temperature-dependent shellfish growth. Secondly, more important environmental factors such as salinity, water depth, bottom type and water velocity (necessary for oyster growing), are not considered. Organic detritus is known to be an important component of bivalve diets (Dame and Patten, 1981; Bayne et al., 1993; Barille et al., 1997), but currently cannot be measured using satellite imagery. Our index therefore provides guidance on suitable water quality conducive to rapid growth, but not sufficient information to model site specific production capacity for suspended or bottom culture.

Although satellite thermal data is only sensitive to the temperature of the top few micrometers of water, and ocean color is sensitive only to one optical depth (which varies, but on the Maine coast is usually the top one or two meters), these data are relevant to the whole water column if the water column is often vertically well-mixed. Indeed, many estuaries on the Maine coast are well-mixed (e.g. the Sheepscot and Medomak Rivers, Thornton and Mayer, 2015; Mayer, 1996), which coincidently qualify for oyster aquaculture in our suitability index (Appendix Table B2). Finally, local knowledge is invaluable for the expansion of an existing industry on the coast of Maine, and stakeholder input is essential for improving such an index with local information such as site accessibility, town ordinances, etc.

4.4. Future Work

Continued sampling during the spring and summer of 2017 will provide a more complete dataset for optimizing ocean color products in Maine. A local algorithm for Landsat 8 Chl *a* along the coast of Maine could be constructed with additional *in situ* samples collected during satellite overpasses. There are several approaches to tune a local algorithm. An empirical approach, such as the OC3 algorithm, uses a relationship between *in situ* measurements and ratios of the satellite sensor bands. A second method involves using a generalized inherent optical properties inversion (GIOP, Werdell et al., 2013). This method solves for Chl *a*, SPM, and CDOM using known spectral shapes of optical properties (for phytoplankton and non-algal absorption and backscattering by particles) and known values of absorbance and backscattering of water (which are weak functions of salinity and temperature). Databases of collection sites located in the Damariscotta River and Harpswell Sound could tune the shapes of inherent optical properties for the GIOP algorithm and provide an estimate of Chl *a* in these two estuaries. Furthermore, *in situ* samples from various locations along the coast will validate the local algorithm so that its use can be expanded from the Damariscotta River to other places along the coast.

Obtaining more parameters from Landsat 8, such as colored dissolved organic matter (CDOM), would provide additional information to growers as well as environmental monitoring and ecosystem managers. Franz et al., (2015) and Slonecker et al., (2015) describe the potential of using Landsat 8 for remote sensing of CDOM in conjunction with *in situ* measurements. A reliable CDOM product would also improve the algorithm for Chl *a*, as the presence of CDOM often contributes to an overestimation of Chl *a*. Furthermore, high levels of CDOM are correlated with low salinity in certain estuaries in Maine (Carder et al., 1989; D'Sa et al., 2002; Mayer, L., 2017 personal communication). It would be helpful to identify areas with significant freshwater influx because these often bring concentrations of bacteria that negatively affect clamming and other fisheries (Kleindinst et al., 2014; Shumway et al., 1988).

CHAPTER 5

CONCLUSION

Our satellite data derived Oyster Suitability Index can act as a powerful tool for oyster aquaculture site selection and the expansion of the shellfish farming industry. It shows that suitable biophysical conditions for oyster growth exist in many areas of the Maine coast. Suitability indices for other bivalve species, such as mussels, scallops, and finfish along the coast, or other applications requiring high spatial resolution, can be developed based on the algorithms presented here. SST, turbidity, and Chl *a* retrieved from Landsat 8 is sufficiently validated by *in situ* matchups (within +/- 1°C for SST; max absolute deviation is 0.96 NTU and relative deviation is 15% for turbidity; and max absolute deviation is 3 μg Chl L^{-1} and relative deviation is 156% for Chl *a*). Our results show that Landsat 8 imagery is useful for retrieving SST, turbidity, and Chl *a* in coastal waters of Maine, USA, and can be applied to other narrow estuaries around the world. The novelty of using Landsat 8 in this context offers a unique opportunity to map and monitor coastal waters at an unprecedented spatial resolution. Inclusion of data from other satellites with complimentary sensor suites such as Sentinel 2A, and the recently launched Sentinel 2B, could improve both the spatial and temporal coverage of coastal waters, as they will provide five-day or better coverage (unfortunately, Sentinel 2A and B do not have thermal bands). SST data from Landsat 8 is especially useful for aquaculture site prospecting. We recommend adding thermal bands to future high resolution missions, as more frequent SST data will assist both site selection for aquaculture and other applications. Future work improving biogeochemical local algorithms, refining the atmospheric correction, and adding other parameters such as CDOM, will further advance the use of high resolution remote-sensing for coastal applications.

REFERENCES

Ahmad, Z., Franz, B. a, McClain, C. R., Kwiatkowska, E. J., Werdell, J., Shettle, E. P., & Holben, B. N. (2010). New aerosol models for the retrieval of aerosol optical thickness and normalized water-leaving radiances from the SeaWiFS and MODIS sensors over coastal regions and open oceans. Applied Optics, 49(29), 5545.

Aguilar Manjarrez, J. & Crespi, V. (2013). FAO Aquaculture Newsletter 55, September 2016.

Barillé, L., Prou, J., Héral, M. and Razet, D., (1997). Effects of high natural seston concentrations on the feeding, selection, and absorption of the oyster Crassostrea gigas (Thunberg). *Journal of experimental marine biology and ecology*, *212*(2), pp.149-172.

Barnes, R. A., Holmes, A. W., & Esaias, W. E. (1995). Stray Light in the SeaWiFS Radiometer. SeaWiFS Technical Report Series, 31(July), 79.

Barnes, T.K., Volety, A.K., Chartier, K., Mazzotti, F.J. and Pearlstine, L., (2007). A habitat suitability index model for the eastern oyster (Crassostrea virginica), a tool for restoration of the Caloosahatchee Estuary, Florida. *Journal of Shellfish Research*, *26*(4), pp.949-959.

Bayne, B.L., Iglesias, J.I.P., Hawkins, A.J.S., Navarro, E., Heral, M. and Deslous-Paoli, J.M., (1993). Feeding behaviour of the mussel, Mytilus edulis: responses to variations in quantity and organic content of the seston. *Journal of the Marine Biological Association of the United Kingdom*, *73*(04), pp.813-829.

Buitrago, J., Rada, M., Hernández, H. and Buitrago, E., (2005). A single-use site selection technique, using GIS, for aquaculture planning: choosing locations for mangrove oyster raft culture in Margarita Island, Venezuela. *Environmental Management*, *35*(5), pp.544- 556.

Cake Jr., E.W., (1983). *Habitat suitability index models: Gulf of Mexico American oyster* (No. 82/10.57). U.S. Fish and Wildlife Service.

Carrasco, M.F. and Barón, P.J., (2010). Analysis of the potential geographic range of the Pacific oyster Crassostrea gigas (Thunberg, 1793) based on surface seawater temperature satellite data and climate charts: the coast of South America as a study case. *Biological Invasions*, *12*(8), pp.2597-2607.

Carder, K. L., Steward, R. G., Harvey, G. R., & Ortner, P. B. (1989). Marine humic and fulvic acids: Their effects on remote sensing of ocean chlorophyll. *Limnology and Oceanography*, *34*(l), 68–81. http://doi.org/10.4319/lo.1989.34.1.0068

Congleton, W.R., Pearce, B.R., Parker, M.R. and Beal, B.F., (1999). Mariculture siting: a GIS description of intertidal areas. *Ecological Modelling*, *116*(1), pp.63-75.

Cullen, J. J. (1982). The deep chlorophyll maximum: Comparing vertical profiles of chlorophyll a. *Canadian Journal of Fisheries and Aquatic Sciences, 39*(5), 791-803. doi:10.1139/f82-108.

Cullen, J.J., (2008). Observation and prediction of harmful algal blooms. In M. Babin, C.S. Roesler and J.J. Cullen [eds.], *Real-time coastal observing systems for ecosystem dynamics and harmful algal blooms*, UNESCO.

Dame, R.F. and Patten, B.C., (1981). Analysis of energy flows in an intertidal oyster reef. *Mar. Ecol. Prog. Ser*, *5*(2), pp.115-124.

D'Sa, E., Hu, C., Muller-Karger, F., & Carder, K. (2002). Estimation of colored dissolved organic matter and salinity fields in case 2 waters using SeaWiFS: Examples from Florida Bay and Florida Shelf. *Journal of Earth System Science, 111*(3) 197-207.

Dogliotti, A. I., Ruddick, K. G., Nechad, B., Doxaran, D., & Knaeps, E. (2015). A single algorithm to retrieve turbidity from remotely-sensed data in all coastal and estuarine waters. *Remote Sensing of Environment*, *156*, 157–168. http://doi.org/10.1016/j.rse.2014.09.020

Donlon, C. J., Minnett, P. J., Gentemann, C., Nightingale, T. J., Barton, I. J., Ward, B., & Murray, M. J. (2002). Toward improved validation of satellite sea surface skin temperature measurements for climate research. *Journal of Climate*, *15*(4), 353–369. http://doi.org/10.1175/1520-0442(2002)015<0353:TIVOSS>2.0.CO;2

Ehrich, M. K., & Harris, L. A. (2015). A review of existing eastern oyster filtration rate models. *Ecological Modelling*, *297*, 201–212. http://doi.org/10.1016/j.ecolmodel.2014.11.023

Epifanio, C.E. and Ewart, J., 1977. Maximum ration of four algal diets for the oyster Crassostrea virginica Gmelin. Aquaculture, 11(1), pp.13-29.

Estapa, M. L., Boss, E., Mayer, L. M., & Roesler, C. S. (2012). Role of iron and organic carbon in mass-specific light absorption by particulate matter from Louisiana coastal waters. *Limnology and Oceanography*, *57*(1), 97–112. http://doi.org/10.4319/lo.2012.57.1.0097

Franz, B. a., Bailey, S. W., Kuring, N., & Werdell, P. J. (2015). Ocean color measurements with the Operational Land Imager on Landsat-8: implementation and evaluation in SeaDAS. *Journal of Applied Remote Sensing*, *9*(1), 96070. http://doi.org/10.1117/1.JRS.9.096070

Gong, C., Chen, X., Gao, F., & Chen, Y. (2012). Importance of weighting for multi-variable habitat suitability index model: A case study of winter-spring cohort of Ommastrephes bartramii in the Northwestern Pacific Ocean. *Journal of Ocean University of China*, *11*(2), 241–248. http://doi.org/10.1007/s11802-012-1898-6

Haven, D.S. and Morales-Alamo, R., 1966. Aspects of biodeposition by oysters and other invertebrate filter feeders. Limnol. Oceanogr, 11(4), pp.487-498.

Hawkins, a. J. S., Pascoe, P. L., Parry, H., Brinsley, M., Cacciatore, F., Black, K. D., … Zhu, M. Y. (2013). Comparative Feeding on Chlorophyll-Rich Versus Remaining Organic Matter in Bivalve Shellfish. *Journal of Shellfish Research*, *32*(3), 883–897. http://doi.org/10.2983/035.032.0332

Hawkins, A.J.S., Pascoe, P.L., Parry, H., Brinsley, M., Black, K.D., McGonigle, C., Moore, H., Newell, C.R., O'Boyle, N., Ocarroll, T. and O'Loan, B., (2013). Shellsim: a generic model of growth and environmental effects validated across contrasting habitats in bivalve shellfish. *Journal of Shellfish Research*, *32*(2), pp.237-253

Hoffmann, E.E., Powell, E.N., Klinck, J.M. and Wilson, E.A. (1992). Modeling oyster populations III. Critical feeding periods, growth. *Journal of Shellfish Research*, *11*(2), pp.399-416.

Holm-Hansen, O., and B. Riemann. (1978). Chlorophyll a determination: improvements in methodology. Oikos, 30: 438-447.

Hudson, A. S., Talke, S. A., & Jay, D. A. (2016). Using Satellite Observations to Characterize the Response of Estuarine Turbidity Maxima to External Forcing. *Estuaries and Coasts*, 1–16. http://doi.org/10.1007/s12237-016-0164-3

Kleindinst, J. L., Anderson, D. M., McGillicuddy, D. J., Stumpf, R. P., Fisher, K. M., Couture, D. A., … Nash, C. (2014). Categorizing the severity of paralytic shellfish poisoning outbreaks in the Gulf of Maine for forecasting and management. *Deep-Sea Research Part II: Topical Studies in Oceanography*, *103*, 277–287. http://doi.org/10.1016/j.dsr2.2013.03.027

Gernez, P., Lerouxel, A., Mazeran, C., Lucas, A., & Barill, L. (2014). Remote sensing of suspended particulate matter in turbid oyster-farming ecosystems. *Journal of Geophysical Research: Oceans*, 7277–7294. http://doi.org/10.1002/2014JC010055.

Loosanoff, V.L., (1958). Some aspects of behavior of oysters at different temperatures. *The Biological Bulletin*, *114*(1), pp.57-70.

Mayer, L. M., University of Maine at Orono., & University of Maine/University of New Hampshire Sea Grant College Program. (1996). *The Kennebec, Sheepscot and Damariscotta River Estuaries: Seasonal oceanographic data*. Orono, Me: Dept. of Oceanography, University of Maine.

McAlice, B. J. (1977). A preliminary oceanographic survey of Damariscotta River Estuary, Lincoln County, Maine. Washington: U.S. National Oceanic and Atmospheric Administration.

Mobley, C. D., Werdell, J., Franz, B., Ahmad, Z., & Bailey, S. (2016). Atmospheric Correction for Satellite Ocean Color Radiometry A Tutorial and Documentation NASA Ocean Biology Processing Group.

Montanaro, M., Gerace, A., Lunsford, A., & Reuter, D. (2014). Stray light artifacts in imagery from the landsat 8 thermal infrared sensor. *Remote Sensing*, 6(11), 10435–10456. http://doi.org/10.3390/rs61110435

NASA. (2016). https://oceancolor.gsfc.nasa.gov/atbd/chlor_a/

Nechad, B., Ruddick, K. G., & Park, Y. (2010). Calibration and validation of a generic multisensor algorithm for mapping of total suspended matter in turbid waters. *Remote Sensing of Environment*, *114*(4), 854–866. http://doi.org/10.1016/j.rse.2009.11.022

Newell, R.I.E. and Jordan, S.J., (1983). Preferential ingestion of organic material by the American oyster Crassostrea virginica. *Marine ecology progress series. Oldendorf*, *13*(1), pp.47-53.

Newell, C.R., S. Shumway, T.L. Cucci and R. Selvin. (1989). The effects of natural seston particle size and type on feeding rates, feeding selectivity and food resource availability for the mussel *Mytilus edulis* Linnaeus, 1758 at bottom culture sites in Maine. J. Shellfish. Res. 8: 187-196.

Newell, C.R., A.J.S. Hawkins, K. Morris, J. Richardson, C. Davis and T. Getchis. (2013). ShellGIS: a dynamic tool for shellfish farm site selection. *World Aquaculture*. 44:50-53.

O'Reilly, J. E., Maritorena, S., Mitchell, B. G., Siegel, D. A., Carder, K. L., Garver, S. A., … McClain, C. R. (1998). Ocean color chlorophyll algorithm for SeaWiFS. *Journal of Geophysical Research*, 103(Cll), 24937–24953.

Pahlevan, N., Lee, Z., Wei, J., Schaaf, C. B., Schott, J. R., & Berk, A. (2014). On-orbit radiometric characterization of OLI (Landsat-8) for applications in aquatic remote sensing. *Remote Sensing of Environment*, *154*, 272–284. http://doi.org/10.1016/j.rse.2014.08.001

Pahlevan, N., Sarkar, S., & Franz, B. A. (2016). Uncertainties in coastal ocean color products: Impacts of spatial sampling. *Remote Sensing of Environment*, *181*, 14–26. http://doi.org/10.1016/j.rse.2016.03.022

Pahlevan, N., Sheldon, P., Peri, F., Wei, J., Shang, Z., Sun, Q., … Loveland, T. (2016). Calibration/validation of landsat-derived ocean colour products in Boston harbour. *International Archives of the Photogrammetry, Remote Sensing and Spatial Information Sciences - ISPRS Archives*, *41*(July), 1165–1168. http://doi.org/10.5194/isprsarchives-XLI-B8-1165-2016

Pérez, O.M., Ross, L.G., Telfer, T.C. and del Campo Barquin, L.M., (2003). Water quality requirements for marine fish cage site selection in Tenerife (Canary Islands): predictive modelling and analysis using GIS. *Aquaculture*, *224*(1), pp.51-68.

Pérez-Camacho, A., Aguiar, E., Labarta, U., Vinseiro, V., Fernández-Reiriz, M.J. and Álvarez-Salgado, X.A., (2014). Ecosystem-based indicators as a tool for mussel culture management strategies. *Ecological Indicators*, *45*, pp.538-548.

Pfannkuche, J., & Schmidt, A. (2003). Determination of suspended particulate matter concentration from turbidity measurements: Particle size effects and calibration procedures. *Hydrological Processes*, 17(10), 1951–1963. http://doi.org/10.1002/hyp.1220

Powell, E.N., Hofmann, E.E., Klinck, J.M. and Ray, S.M., (1992). Modeling oyster populations 1. A commentary on filtration rate. Is faster always better? *J. Shellfish Res*., 1 I: 387-398.

Radiarta, I. N., Saitoh, S. I., & Miyazono, A. (2008). GIS-based multi-criteria evaluation models for identifying suitable sites for Japanese scallop (Mizuhopecten yessoensis) aquaculture in Funka Bay, southwestern Hokkaido, Japan. *Aquaculture*, *284*(1–4), 127–135.

Rasmussen, J. B., Godbout, L., & Schallenburg, M. (1989). The humic content of lake water and its relationship to watershed and lake morphometry. *Limnology and Oceanography*, 34(7), 1336-1343.

Rheault, R. B., & Rice, M. A. (1996). Food-limited growth and condition index in the eastern oyster, Crassostrea virginica (Gmelin 1791), and the bay scallop, Argopecten irradians irradians (Lamarck 1819). *Journal of Shellfish Research*, *15*(2),

Roesler, C., & Culbertson, C. (2016). Lake Transparency : A Window into Decadal Variations in Dissolved Organic Carbon Concentrations in Lakes of Acadia National. http://doi.org/10.1007/978-3-319-30259-1

Shumway, S. E., Sherman-Caswell, S., & Hurst, J. (1988). Paralytic shellfish poisoning in Maine: monitoring a monster. *Journal of Shellfish Research*.

Siegel, D. A., Maritorena, S., Nelson, N. B., & Behrenfeld, M. J. (2005). Independence and interdependencies among global ocean color properties: Reassessing the bio-optical assumption. *Journal of Geophysical Research C: Oceans*, *110*(7), 1–14. http://doi.org/10.1029/2004JC002527

Slonecker, E. T., Jones, D. K., & Pellerin, B. A. (2015). The new Landsat 8 potential for remote sensing of colored dissolved organic matter (CDOM). *Marine Pollution Bulletin*, *107*(2), 518–527. http://doi.org/10.1016/j.marpolbul.2016.02.076

Soniat, T.M. and Brody, M.S., (1988). Field validation of a habitat suitability index model for the American oyster. *Estuaries and Coasts*, *11*(2), pp.87-95.

Thomas, A., Byrne, D., and Weatherbee, R. (2002). Coastal sea surface temperature variability from Landsat infrared data. *Remote Sens. Environ*. *81*, 262–272.

Thomas, Y., Mazurié, J., Alunno-Bruscia, M., Bacher, C., Bouget, J. F., Gohin, F., … Struski, C. (2011). Modelling spatio-temporal variability of Mytilus edulis (L.) growth by forcing a dynamic energy budget model with satellite-derived environmental data. *Journal of Sea Research*, *66*(4), 308–317. http://doi.org/10.1016/j.seares.2011.04.015

Thompson, B. P., & Perry, M. J. (2006). Temporal and Spatial Variability of Phytoplankton Biomass in the Damariscotta River Estuary, Maine, USA. *Department of Marine Sciences*, *Master of*.

Thornton, K., & Mayer, L. (2015). Maine Coastal Observing Alliance, Summary Report 2014.

Tissot, C., Brosset, D., Barillé, L., Le Grel, L., Tillier, I., Rouan, M. and Le Tixerant, M., (2012). Modeling oyster farming activities in coastal areas: a generic framework and preliminary application to a case study. *Coastal Management*, 40(5), pp.484-500.

USGS. (2016). L8 OLI/TIRS product. https://earthexplorer.usgs.gov

Vanhellemont, Q., & Ruddick, K. (2014). Turbid wakes associated with offshore wind turbines observed with Landsat 8. *Remote Sensing of Environment*, *145*, 105–115.

Wang, H., Hladik, C. M., Huang, W., Milla, K., Edmiston, L., Schalles, J. F., … Edmiston, L. (2010). Detecting the spatial and temporal variability of chlorophyll-a concentration and total suspended solids in Apalachicola Bay , Florida using MODIS imagery. *International Journal of Remote Sensing*, *1161*(December 2016). http://doi.org/10.1080/01431160902893485

Wang, P., Boss, E. S., & Roesler, C. (2005). Uncertainties of inherent optical properties obtained from semianalytical inversions of ocean color. *Applied Optics*, *44*(19), 4074–4085. http://doi.org/10.1364/AO.44.004074

Ward, B. (2006). Near-surface ocean temperature. *Journal of Geophysical Research: Oceans*, *111*(2), 1–18. http://doi.org/10.1029/2004JC002689

Widdows, J., Fieth, P. and Worrall, C.M., (1979). Relationships between seston, available food and feeding activity in the common mussel Mytilus edulis. *Marine Biology*, *50*(3), pp.195-207.

APPENDIX A: ASSESSMENT OF ATMOSPHERIC CORRECTION

Water samples with high CDOM (measured with a Cary-50) and low turbidity (measured with a Hach-3) were used to verify the selection of a freshwater pond as a target with insignificant reflectance in the blue following an atmospheric correction.

Beginning with a relationship between $R_{rs}(443)$, and the absorption and backscattering coefficients (e.g. Wang et al., 2005) of water (subscript w), dissolved substances (subscript g) and particulate substances (subscript p):

$$R_{rs}(443) = 0.095 * \frac{b_{bw}(443)+b_{bp}(443)^{*}}{a_w+a_g(443)+a_p{}^{*}(443)+b_{bw}(443)+b_{bp}(443)^{*}} \quad \text{(A1)}$$

We measured during the summer of 2016 the absorption coefficient and turbidity of two humic ponds (Biscay and Muddy ponds, Table A1). Together with values of water absorption and backscattering from the literature (Table A2) and relationship between particulate properties and turbidity, we derived reflectance values (Table A1) that are not significantly different from zero given Landsat 8 signal to noise ratio (Pahlevan et al., 2016).

Table A1 Measured Values in Humic Pond

Variable	Biscay Pond	Muddy Pond
$a_g(443)$ [m^{-1}]	4.4	7.0
T [NTU]	2.3	8.7
$R_{rs}(443)$ [sr^{-1}]	7.29*10^{-4}	4.56*10^{-4}

Table A2 Values from literature for equation (A1)

absorption of water	$a_w(443)$	0.006	(Sullivan et al. 2006, Mason et al. 2016)
mass specific absorption	$a_p{}^*(443)$	0.06 m^2/g	(Estapa et al., 2012, Figure 3)
backscattering of inorganic particles	$b_{bp}{}^*(443)$	0.034	(b_{bp}= (0.03)T; Twardowski et al., 2001)
backscattering of water	b_{bw}(443)	0.003	(Zhang et al. 2009)

Table A3

Dilution series of Arizona Dust standard with Hach and LOBO WQM turbidity measurements.

AZ dust added [ml]	Hach [NTU]	Buoy Sensor [NTU]
0	2.26	0.85
2	4.39	1.77
4	7.29	2.87
7	10.43	4.38
15	18.93	6.46

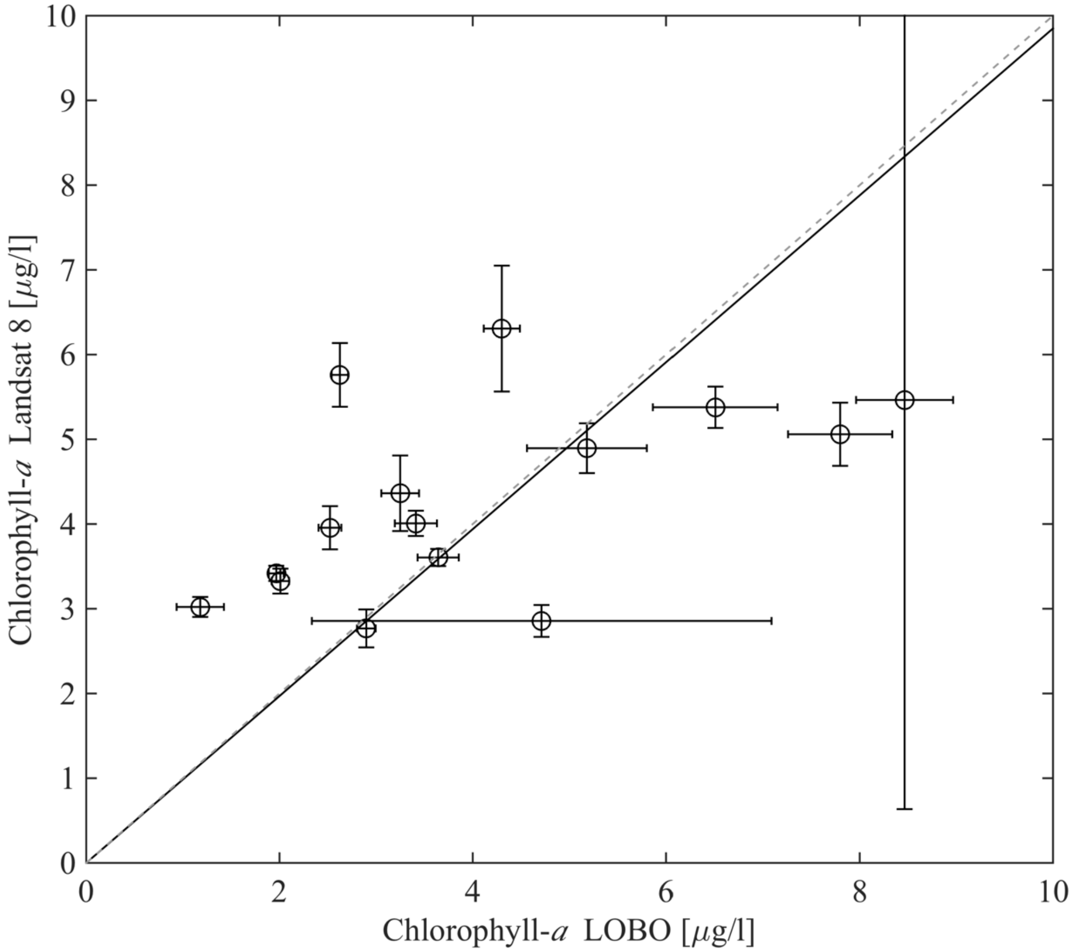

Figure A1. Type II linear regression between Landsat 8 chlorophyll-a and chlorophyll-a measured by LOBO buoys at night time. Vertical error bars are the standard deviation about a 5x5 pixel box. Horizontal error bars are the standard deviation of chlorophyll for four hours at each buoy. Buoy chlorophyll-a was corrected by chlorophyll extraction samples with a slope factor or 1.71. Root mean square error is 1.0 µg Chl l^{-1}, r^2= 0.31 and the grey line is 1:1.

APPENDIX B. OYSTER SUITABILITY INDEX

Table B1

Criteria for Oyster Suitability Index. The weights are additive, except when at least one parameter has poor conditions, in which case the entire criteria is then multiplied by zero.

Physical parameter	Ideal conditions (1)	Moderate conditions (.6)	Poor conditions (0)	Importance factor
SST [˚C]	SST > 22	22 > SST > 20	20 > SST	0.8
Turbidity [NTU]	8 > Turbidity	10 > Turbidity > 8	Turbidity > 10	0.05
Chl *a* [µg/l]	10 > Chl *a* > 3	3 > Chl *a* > 1	1 > Chl *a* Chl *a* > 10	0.15

Table B2

Oyster Suitability Index scores and average July SST at existing and prospective oyster aquaculture sites in Maine.

	Upper Damariscotta River	Medomak	Maquoit Bay	New Meadows	Upper Sheepscott River	Cousins Island
OSI score	0.94	0.90	1.0	0.84	0.84	0.78
SST [˚C]	24	22	23	24	22	22

APPENDIX C. AVERAGED MONTHLY SATELLITE DATA

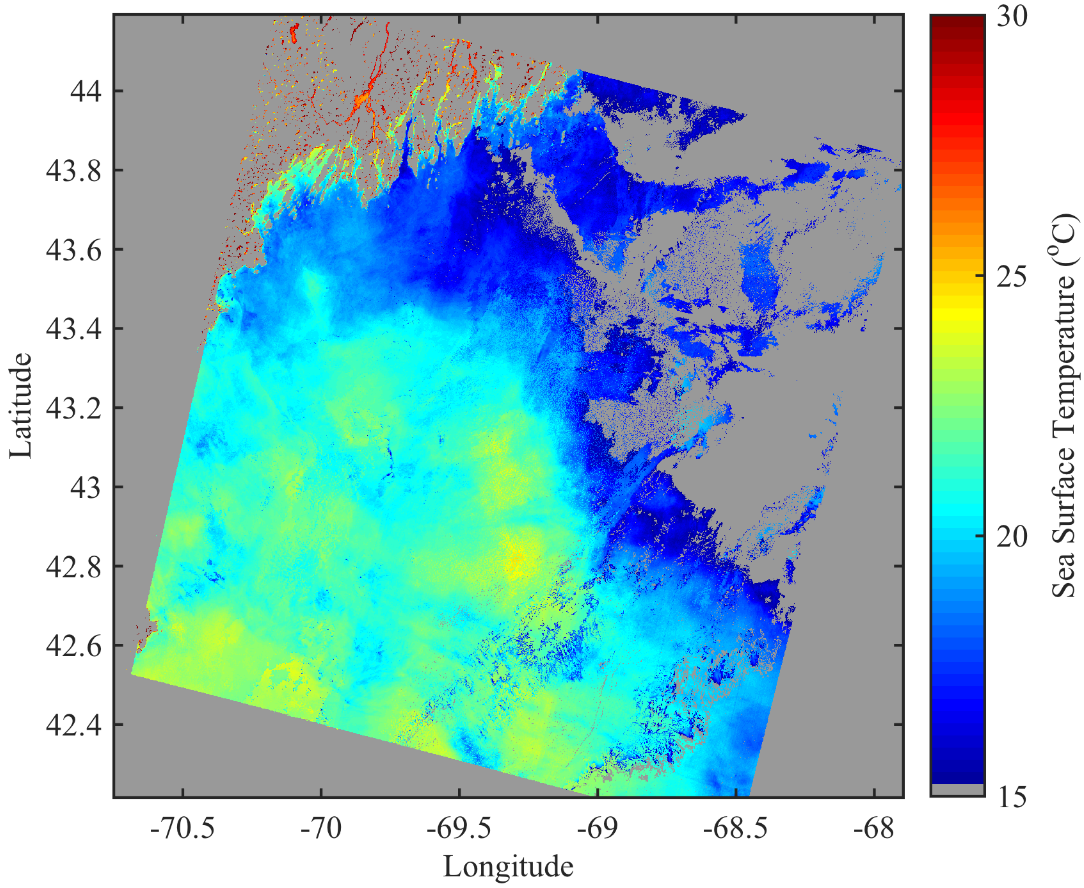

Figure C.1. Sea surface temperature derived from Landsat 8 data averaged over all images in July from 2013 to 2016.

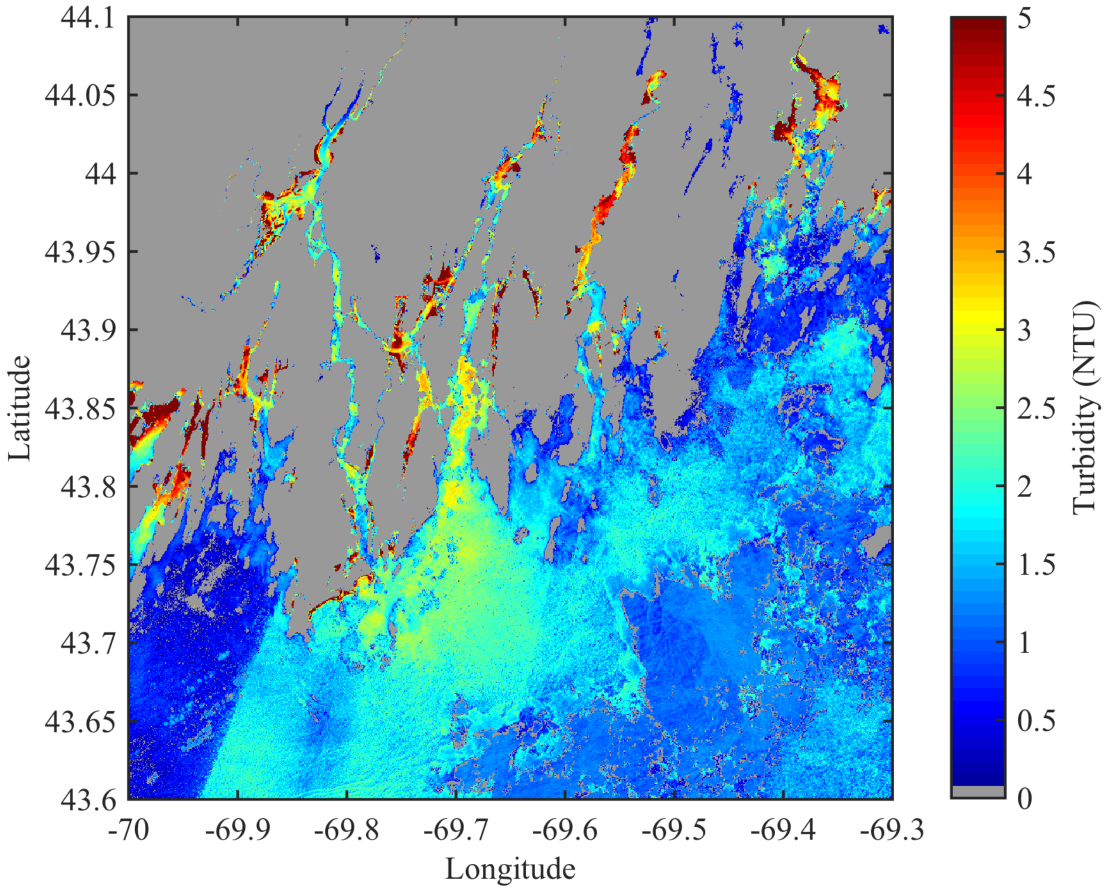

Figure C.2. Turbidity derived from Landsat 8 data averaged over all images in July from 2013 to 2016.

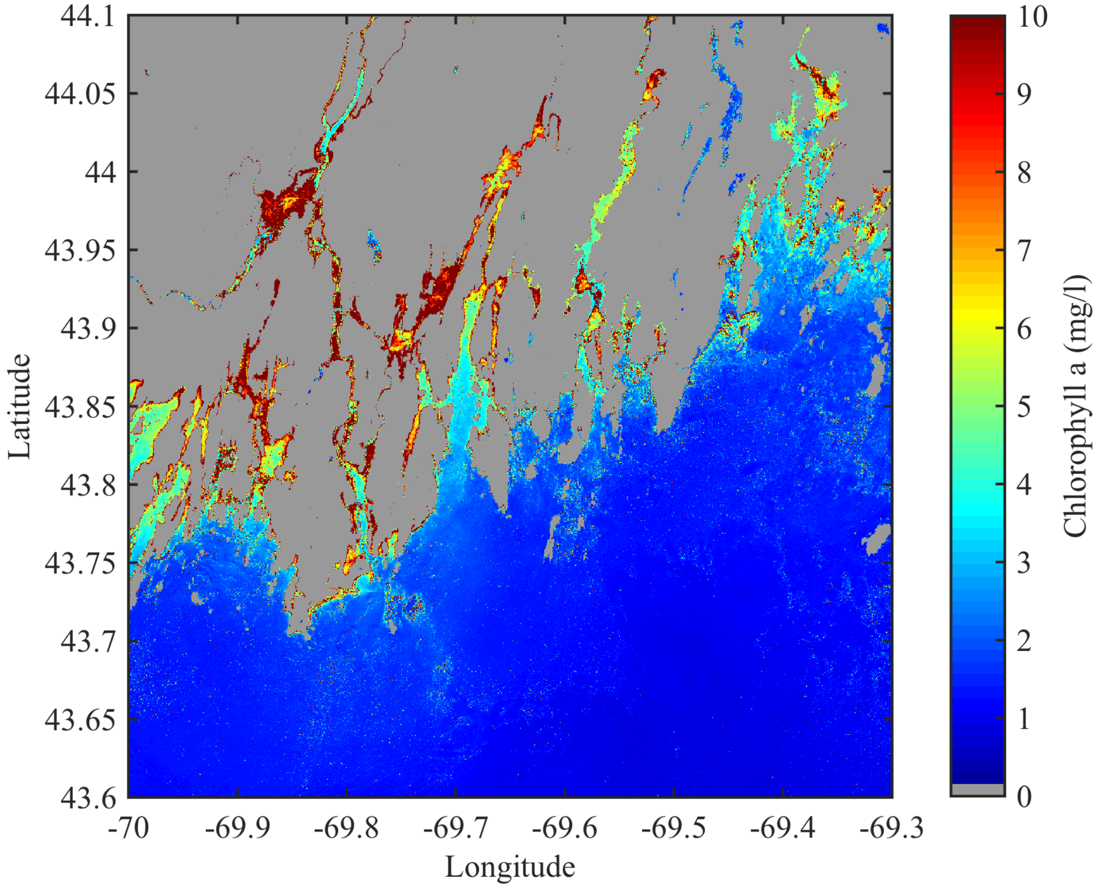

Figure C.3. Chlorophyll a derived from Landsat 8 data averaged over each image in July from 2013 to 2016.

APPENDIX D. STANDARD DEVIATION OF MONTHLY CLIMATOLOGY MAPS

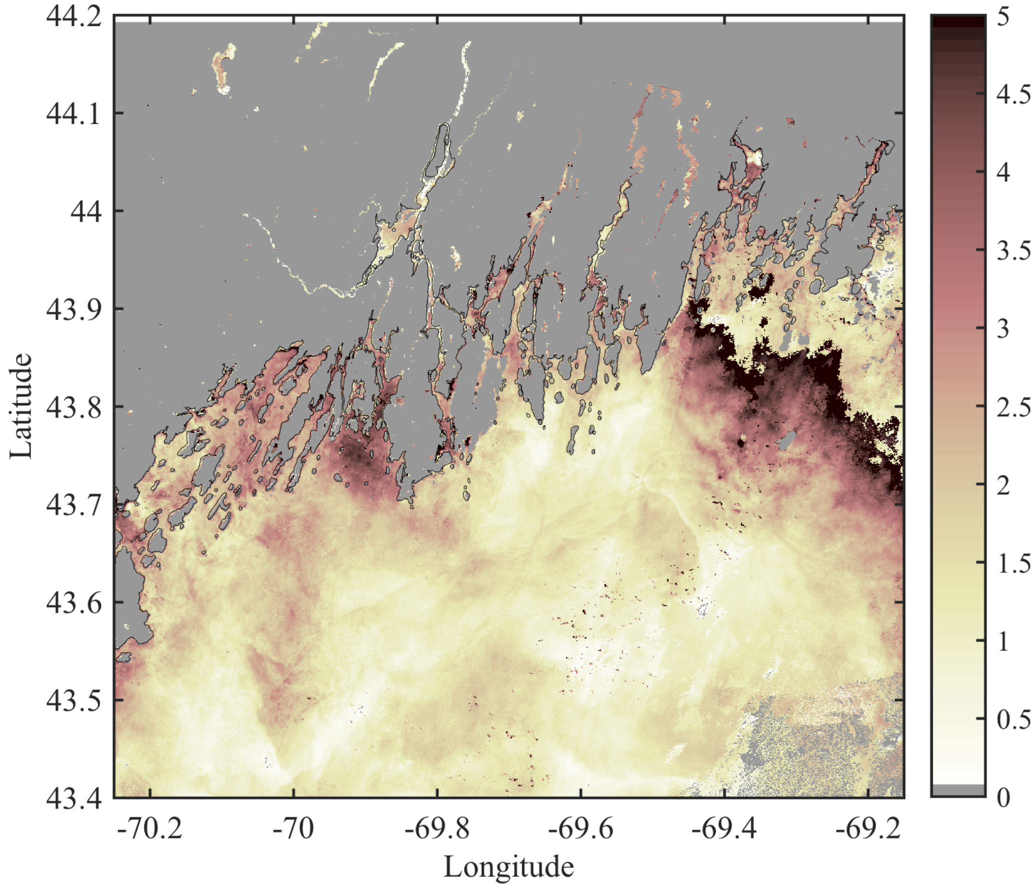

Figure D.1. Standard deviation of monthly averaged sea surface temperature data in July from 2013 to 2016. Higher variability near river mouths indicate differences in temperature due to riverine output. Dark areas may be poorly masked clouds or atmospheric artifacts.

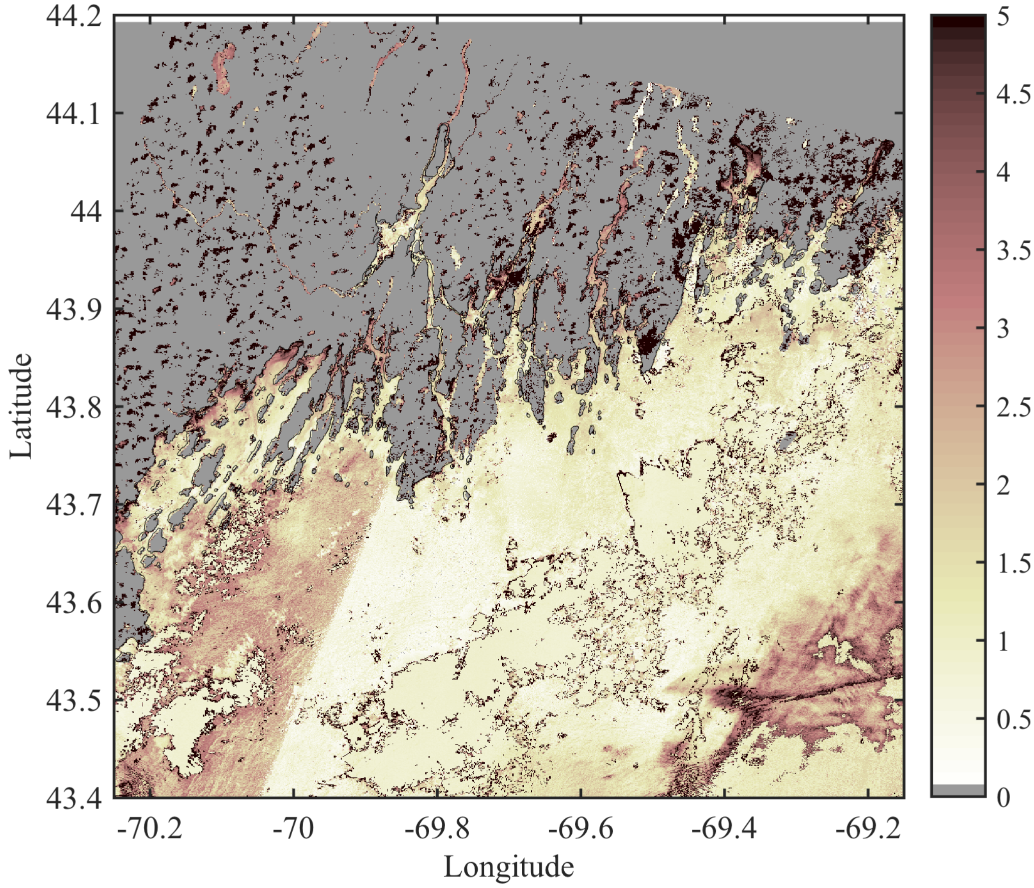

Figure D.2. Standard deviation of monthly averaged turbidity data in July from 2013 to 2016. High variability in the bottom left corner reveal a striping effect in one of the four compiled images. Dark areas may be poorly masked clouds or atmospheric artifacts.

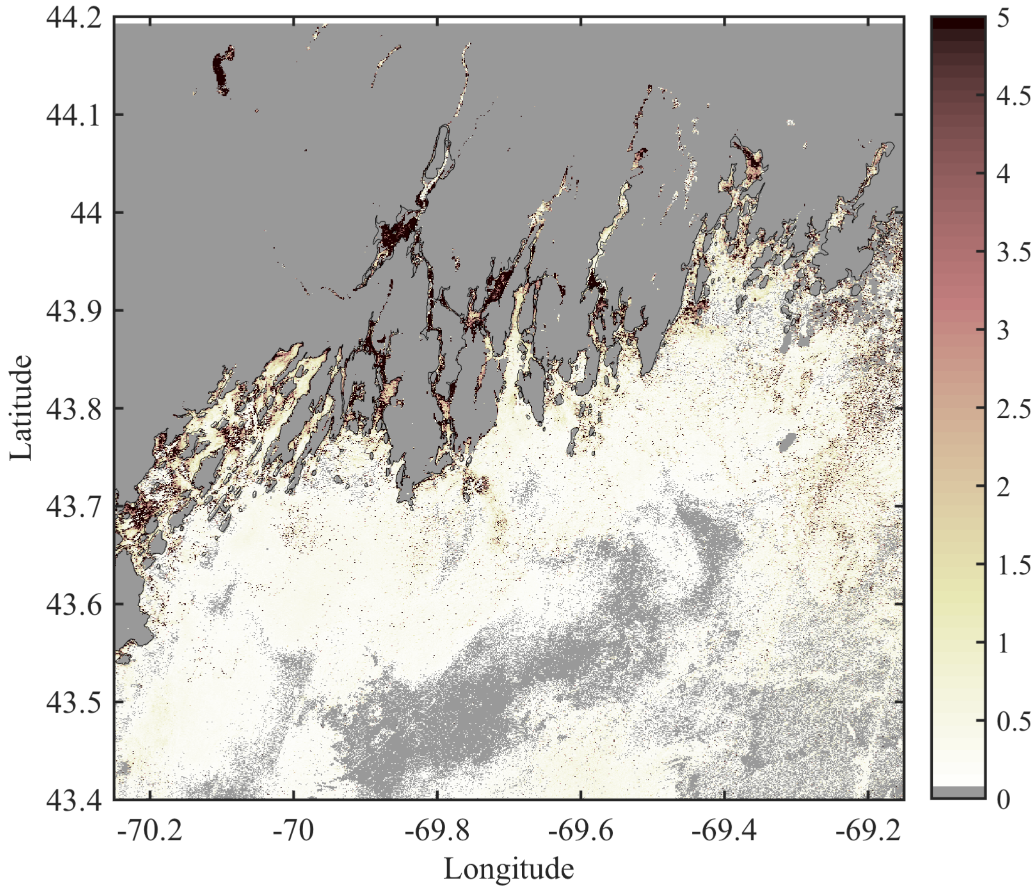

Figure D.3. Standard deviation of monthly averaged chlorophyll a data in July from 2013 to 2016. Variability of chlorophyll a in the upper estuaries is higher than variability of chlorophyll a offshore.

BIOGRAPHY OF THE AUTHOR

Jordan Snyder was born in Anaheim, California on December 13, 1990. She was raised in Huntington Beach, California and graduated from Huntington Beach High School in 2009. She attended the University of California, Davis and graduated in 2013 with a Bachelor's degree in Geology. She moved to Maine and entered the Oceanography graduate program at The University of Maine in the summer of 2015. She enjoys surfing, SCUBA diving, running, hiking, camping, gardening, cooking and laughing. Jordan is a candidate for the Master of Science degree in Oceanography from the University of Maine in August 2017.